JOURNAL OF PETROLOGY | VOLUME 50 | NUMBER 5 | PAGES 841–873 | 2009 | doi:10.1093/petrology/egp022

Generation of Tonalitic and Dioritic Magmas by Coupled Partial Melting of Gabbroic and Metasedimentary Rocks within the Deep Crust of the Famatinian Magmatic Arc, Argentina

JUAN E. OTAMENDI[1]*, MIHAI N. DUCEA[2], ALINA M. TIBALDI[1], GEORGE W. BERGANTZ[3], JESÚS D. DE LA ROSA[4] AND GRACIELA I. VUJOVICH[5]

[1]DEPARTAMENTO DE GEOLOGÍA, UNIVERSIDAD NACIONAL DE RÍO CUARTO, X5804BYA RIO CUARTO, ARGENTINA

[2]DEPARTMENT OF GEOSCIENCES, UNIVERSITY OF ARIZONA, TUCSON, AZ 85721, USA

[3]DEPARTMENT OF EARTH AND SPACE SCIENCES, UNIVERSITY OF WASHINGTON, SEATTLE, WA 98195-1310, USA

[4]DEPARTAMENTO DE GEOLOGÍA, UNIVERSIDAD DE HUELVA, E21071 HUELVA, SPAIN

[5]DEPARTAMENTO DE CIENCIAS GEOLÓGICAS, UNIVERSIDAD DE BUENOS AIRES, 1428 BUENOS AIRES, ARGENTINA

RECEIVED AUGUST 18, 2008; ACCEPTED MARCH 27, 2009
ADVANCE ACCESS PUBLICATION MAY 8, 2009

The source regions of dioritic and tonalitic magmas have been identified in a deep crustal section of the Famatinian arc (Sierras Pampeanas of western Argentina). The source zones of intermediate igneous rocks are located at the transition between a gabbro-dominated mafic unit and a tonalite-dominated intermediate unit. In the upper levels of the mafic unit mafic magmas intruded into metasedimentary wall-rocks, crystallized mainly as amphibole gabbronorite and caused the partial melting of the surrounding metasediments. In turn, the leucogranitic melts sourced from the metasedimentary rocks intruded into the newly crystallized but still hot mafic layers and catalysed the process of partial melting of the gabbroic plutonic rocks. The gabbroic rocks became mafic migmatites comprising amphibole-rich pyroxene-bearing mesosomes and leucotonalitic veins. Significantly, most of the mafic migmatites have isotopic compositions [$^{87}Sr/^{86}Sr(T) < 0{\cdot}7063$ and $\varepsilon_{Nd}(T) = -0{\cdot}94$ to $+2{\cdot}24$] similar to those of the gabbroic rocks and distinct from those of their complementary leucotonalitic veins [$^{87}Sr/^{86}Sr(T) = 0{\cdot}7075$–$0{\cdot}7126$ and $\varepsilon_{Nd}(T) < -2{\cdot}65$], providing evidence for the idea that melting of the mafic rocks was triggered by the intrusion of leucogranitic anatectic melts [$^{87}Sr/^{86}Sr(T) = 0{\cdot}715$ and $\varepsilon_{Nd}(T) = -6{\cdot}21$]. Mass-balance calculations show that the model reaction plagioclase + amphibole + leucogranitic melt → leucotonalitic melt + clinopyroxene ± orthopyroxene can better explain the partial melting of the gabbroic rocks. Based on field observations, we argue that the coalescence of leucotonalitic veins in the mafic migmatites led to breakdown of the solid matrix to form melt-dominated leucotonalitic pools. However, the leucotonalitic veins that crystallized before leaving behind the mafic migmatitic rock are chemically (elemental and isotopic) more evolved than the dioritic and tonalitic rocks. We envisage that once detached from their source region the leucotonalitic magmas were able to react, commingle and mix with entrained fragments of both mafic and metasedimentary rocks. This process gave rise to melts that became tonalitic and dioritic magmas. This study concludes that the generation of intermediate magmas is a multistage process with three critical steps: (1) influx and emplacement of hydrous mafic magmas into a deep crust containing metasedimentary country rocks; (2) physically and chemically coupled melting of mafic and metasedimentary rocks, leading to the formation of a leucotonalitic vein and dyke system that coalesces to form leucotonalitic or tonalitic magma bodies; (3) retrogression of the leucotonalitic magmas by partially assimilating entrained fragments of their mafic and metasedimentary precursors. The dimensions of the

*Corresponding author. E-mail: jotamendi@exa.unrc.edu.ar

source zone seem to be insufficient to generate crustal-scale volumes of intermediate igneous rocks. However, the Famatinian paleo-arc crust would expose only those magma source zones that were still active during the tectonic closure of the arc. Ultimately, a time-integrated perspective indicates that early active source zones were cannibalized during the downward expansion of the plutonic bodies already dominated by intermediate plutonic rocks.

KEY WORDS: *magma genesis; partial melts; plutonic rocks; active continental margin; Famatinian arc*

INTRODUCTION

The origin of calc-alkaline intermediate igneous rocks in magmatic arcs involves interaction between several different magma sources (Eichelberger, 1978; Hildreth & Moorbath, 1988; Collins, 1996; Davidson *et al.*, 1998; among others). The contributing sources include: (1) fluids and melts released by the subducted slab that metasomatize the overriding asthenospheric mantle wedge, with the consequent formation of primary subduction-related melts (Tatsumi & Eggins, 1995); (2) the lithospheric mantle, where the ascending primary magmas re-equilibrate with their ultramafic wall-rocks (Parkinson *et al.*, 2003); (3) the crust, where mantle-derived magmas interact with either older igneous rocks or accretionary metasedimentary sequences (Eichelberger, 1978; Davidson *et al.*, 1988; Hildreth & Moorbath, 1988). The view that intermediate magmas result from petrological processes involving multiple-contributing sources is now fairly well constrained in both plutonic and eruptive environments (e.g. DePaolo, 1981; Gray, 1984; Collins, 1996; Reiners *et al.*, 1996; Barnes *et al.*, 2002; Davidson *et al.*, 2005). Because the great majority of the intermediate magmas have a mantle-derived igneous precursor, it has been hypothesized that petrological processes such as partial melting and fractional crystallization are the causal mechanisms linking intermediate magmas with their parental igneous precursor (Gill, 1981; Grove & Kinzler, 1986; Gromet & Silver, 1987; Atherton & Petford, 1993; Tepper *et al.*, 1993). Additionally, mantle-derived magmas can assimilate crustal rocks while residing at deep crustal levels and evolving under high ambient temperature and pressure (Davidson *et al.*, 1988; Hildreth & Moorbath, 1988; Patiño Douce, 1995; Barnes *et al.*, 2002). Sparks (1986) provided evidence for the existence of crustal contamination in igneous rocks with Precambrian to modern ages; more recently, Annen & Sparks (2002) showed that crustal-scale mixtures of hydrous juvenile magmas and fertile sedimentary packages can yield intermediate and silicic magmas and that the process satisfies thermo-physical constraints.

Current hypotheses about the processes that govern the generation of intermediate subalkaline magmas have been largely based on chemical—elemental and isotopic—variations observed in volcanic and epizonal plutonic rocks (Gromet & Silver, 1987; Davidson *et al.*, 1988; Hildreth & Moorbath, 1988; DePaolo *et al.*, 1992; Atherton, 1993; Chappell, 1997; Gamble *et al.*, 1999; Feeley *et al.*, 2008; among others). Much of the progress in understanding the contributions to the diversity of arc magmatism from deeper levels has come from indirect methods such as integrating xenolith studies (Ducea & Saleeby, 1996; Arai & Kida, 2000; Dungan & Davidson; 2004; Lee *et al.*, 2006) and geophysical data (Rudnick & Fountain, 1995; Zandt *et al.*, 2004). Further understanding of the petrological processes that operate in the deep crust of magmatic arcs requires observations of geological sequences exposing the lower crustal levels of 'ancient' magmatic arcs. This approach has been applied to lower–middle crustal sections formed in magmatic arcs, among which prominent Phanerozoic examples are the Talkeetna Arc section in Alaska (DeBari & Coleman, 1989; Greene *et al.*, 2006), the Kohistan Arc in the NW Himalayas (Garrido *et al.*, 2006; Jagoutz *et al.*, 2007), Fiordland in New Zealand (Muir *et al.*, 1998), the southern Sierra Nevada, California (Saleeby, 1990; Pickett & Saleeby, 1993), the Salinian block in the Santa Lucia Mountains in central California (Ducea *et al.*, 2003; Kidder & Ducea, 2006), parts of the Coast Mountains batholith in British Columbia (Hollister & Andronicos, 2006), and the Famatinian arc in northwestern Argentina (DeBari, 1994; Otamendi *et al.*, 2009).

This study presents a novel mechanism for the petrogenesis of dioritic and tonalitic rocks found in middle to lower crustal section of the Famatinian magmatic arc. We provide observational evidence for coupled partial melting of gabbroic and metasedimentary rocks during the development of this deep arc crustal section. We use field relationships and petrography with mineral and whole-rock chemical and isotopic data to show that the generation of intermediate magma was triggered by the intrusion of hydrous mafic magmas into metasedimentary sequences that resulted in the generation of intermediate magma bodies. These results have important implications for the interpretation of the compositional variation found in both volcanic fields and plutonic igneous rocks emplaced at shallow crustal depths in subduction-related settings.

GEOLOGICAL SETTING

The Famatinian arc

The Famatinian magmatic arc in western Argentina is a differentially exhumed section of a Late Cambrian–Middle Ordovician arc formed by plate subduction beneath the Gondwanan margin (Toselli *et al.*, 1996; Pankhurst *et al.*, 1998). The Famatinian arc is exposed along a distance of more than 1500 km within different segments of the modern central Andean orogen; the transition from plutonic to volcanic Famatinian rocks can be followed

over large regions in northwestern Argentina (Rapela *et al.*, 1992; Toselli *et al.*, 1996; Pankhurst *et al.*, 1998; Coira *et al.*, 1999). The deepest plutonic levels of the arc are exposed in areas where the Nazca plate is currently subducting at a relatively low angle (Barazangi & Isacks, 1976). The deep-seated crustal levels of the Famatinian arc form a wide, roughly north–south-striking, belt extending for about 600 km between 28° and 33°S (Fig. 1). Ordovician eruptive rocks are interbedded with sedimentary rocks in the Puna–Altiplano region between 22° and 28°S (Coira *et al.*, 1999) and in the Famatina Mountains (Mannhein & Miller, 1996; Fanning *et al.*, 2004). The wall-rocks of all the Famatinian batholiths are metasedimentary packages largely consisting of siliciclastic sediments with subordinate interlayered carbonate beds (Caminos, 1979). This regional-scale package of sedimentary rocks experienced metamorphism at a time broadly synchronous with the igneous activity, under either contact aureole or regional Barrovian-type regimes (e.g. Pankhurst *et al.*, 2000, and references therein). As progressively deeper levels of the Famatinian paleo-arc crust are exposed southwards along strike, Neoproterozoic to Early Ordovician stratigraphic units that predate the Famatinian subduction-related magmatism are continuously mapped, ranging from non- to weakly metamorphosed sedimentary rocks in the Puna area to regional and contact metamorphosed metasedimentary rocks in the central Sierras Pampeanas (Aceñolaza *et al.*, 2000). Thick Late Neoproterozoic–Early Cambrian turbiditic packages of the Puncoviscana Formation (e.g. Ježek *et al.*, 1985) and Late Cambrian shallow marine sediments make up the most voluminous protoliths to the metamorphic units hosting the Famatinian arc plutonic rocks. Epizonal plutons in the Famatina Mountains and neighbouring areas are, however, intruded into early Ordovician volcano-sedimentary sequences formed during an early magmatic arc stage (Toselli *et al.*, 1996; Astini & Dávila, 2004).

The Sierra Valle Fértil

The Valle Fértil mafic–intermediate plutonic complex of Ordovician age (K. Stair & M. N. Ducea, unpublished data), is located in the western region of the Famatinian magmatic arc within the Sierras Pampeanas of northwestern Argentina (Figs 1 and 2). The Sierra Valle Fértil contains well-exposed sections showing the transition between lower-crustal and upper-crustal levels (Otamendi *et al.*, 2008). Field and petrological studies allow us to infer the position of the various rock units at the time of active magmatism (Mirré, 1976; Vujovich *et al.*, 1996; Otamendi *et al.*, 2009). In this reconstruction, the upper part of the section corresponds to its eastern boundary, whereas deeper levels of the Ordovician crust are exposed to the west. From west to east, the igneous lithologies display a progression towards more silicic compositions. Each lithological unit, defined by the predominance of one rock type, is mappable at a kilometre scale, but petrographic variations within a unit encompass several rock types (Otamendi *et al.*, 2009). In general terms, the 'stratigraphy' can be described in terms of four units, as follows.

(1) A mafic unit dominated by amphibole gabbronorites and Qtz-poor diorites, and including mafic and ultramafic olivine-bearing cumulate rocks. Although some mafic rocks preserve pristine non-cumulate or cumulate igneous textures from outcrop to microscopic scales, the majority of the gabbroic rocks have granoblastic textures and a granulite-like appearance.

(2) An intermediate unit comprising an extremely heterogeneous suite of amphibole-rich and biotite-bearing tonalites. This tonalitic-dominated unit is in some places separated from the mafic unit by a migmatite-dominated belt.

(3) A granodioritic igneous unit consists of biotite ± amphibole-bearing granodiorites that at a regional scale form a batholith (Fig. 2). The contact between the tonalite-dominated and the granodioritic batholith is transitional, occupies a 2 km wide belt, and contains a mixture of tonalitic, granodioritic and leucogranitic rocks. In the Sierra Valle Fértil, emplacement of voluminous tonalites and granodiorites took place between 490 and 465 Ma during the most active magmatic time in the Famatinian arc (e.g. Pankhurst *et al.*, 2000; Stair *et al.*, 2007).

(4) A metasedimentary unit dominated by paragneissic migmatites (metatexite ≫ diatexite) that occur as kilometre-long belts intercalated with mafic and intermediate igneous rocks or appear widespread as metre-long fragments in all three igneous units. Among the metasedimentary rocks, only thick beds of quartzofeldpathic gneiss do not show any evidence of having experienced partial melting (Otamendi *et al.*, 2008). Instead, most metasedimentary migmatites are characterized by a well-developed layering that results from the alternation of Qtz + Bt + Pl ± Grt ± Crd [abbreviations for minerals are after Kretz (1983)] mesosomes and leucogranitic leucosomes. Tabular leucogranite bodies ranging in width from 5 cm to tens of metres are found within and outside the metasedimentary migmatites, but have been mapped as part of the metasedimentary unit (Otamendi *et al.*, 2009). This unit also consists of subordinate amounts of marble, amphibolite and calcsilicate rocks that locally form kilometre-scale lensoid bodies within the tonalites and granodiorites. Metapelitic and semipelitic migmatites interlayered in the mafic unit record peak metamorphic pressures between 5·2 and 7·1 kbar at granulite-facies temperatures of around 805 ± 35°C (Otamendi *et al.*, 2008).

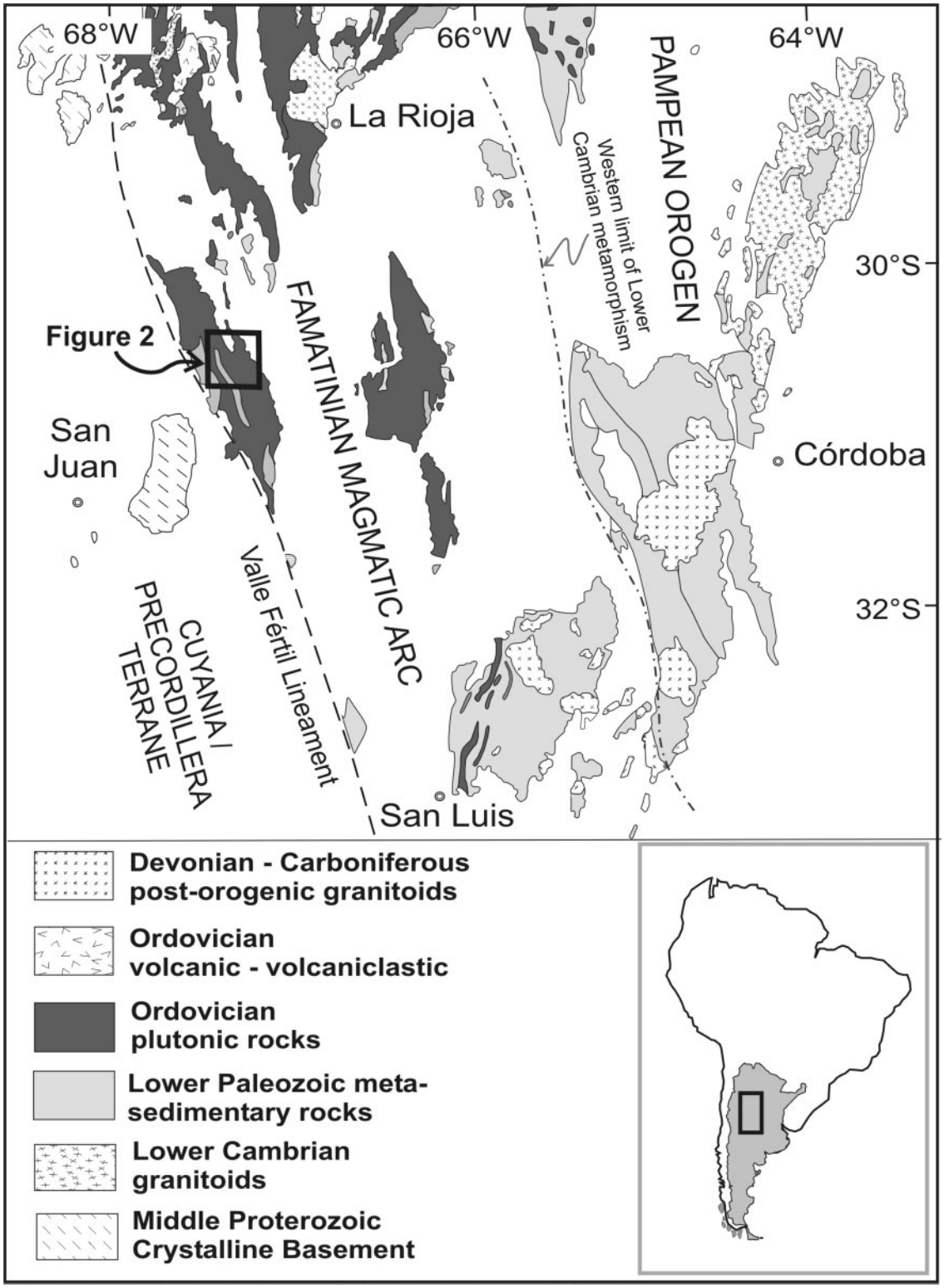

Fig. 1. Geological map showing the central segment of the Famatinian magmatic arc and its location with respect to the Early Cambrian Pampean orogen, and the Laurentia-derived Cuyania and/or Precordillera terrane, based on references given in the text. Inset shows the location of the study area in Argentina.

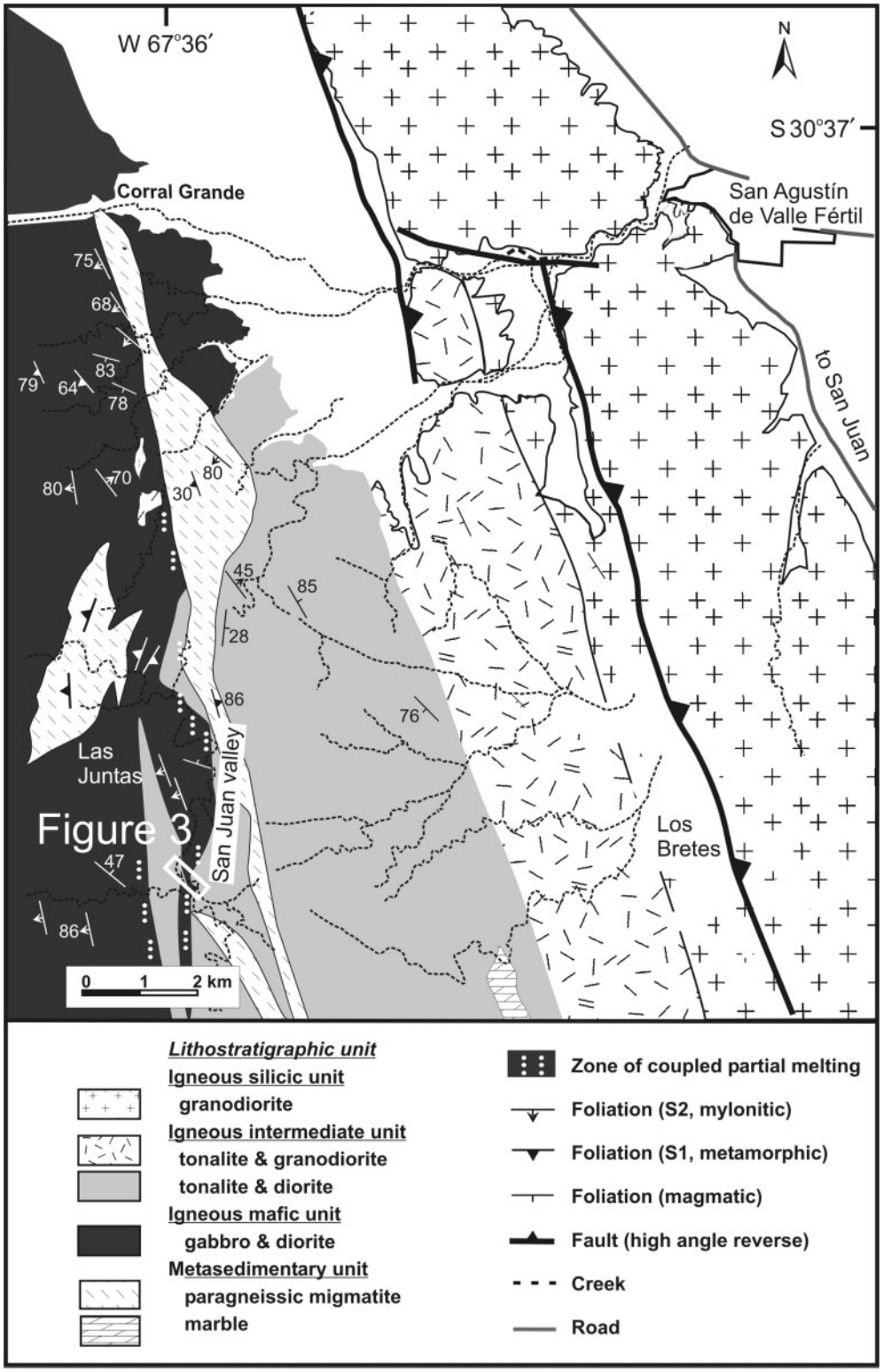

Fig. 2. Geological map of the central section of the Sierra de Valle Fértil (see Fig. 1 for location) based on detailed field mapping and previously published maps (e.g. Mirré, 1976).

FIELD RELATIONS AND PETROGRAPHY

Some of the best-preserved sections that reveal the transition between the mafic and intermediate units in the Sierra de Valle Fértil are found along the San Juan Valley (Fig. 2). A regional-scale geological feature also found here is a sequence of metasedimentary granulite-facies rocks that form well-defined linear belts interlayered with the gabbroic rocks of the mafic unit. Metasedimentary migmatites occur exclusively as blocky, partially assimilated fragments within the dioritic and tonalitic bodies of the intermediate unit (Fig. 3). Below we characterize the field relationships and petrographic observations that are essential to the interpretation of the petrogenesis of the studied rocks (see Table 1).

Mafic unit

Gabbro, mafic migmatite and leucotonalitic veins

The gabbroic rocks show alternations of supra-solidus magmatic and sub-solidus textures at all scales (millimetres to metres). Up to a few centimetres thick magmatic layering, if present, is defined by the alternation of plagioclase-poor and plagioclase-rich bands. The magmatic texture is medium-grained, hypidiomorphic and equigranular with elongated, aligned and clustered grains of hornblende, orthopyroxene and plagioclase. Gabbroic rocks consist of hornblende, orthopyroxene, plagioclase, magnetite and ilmenite, with sporadic clinopyroxene (specimen VFSJ10; the rock sample labels are those utilized in the tables and figures). Most of the gabbroic rocks are hornblende gabbros composed of similar amounts of hornblende [X_{Mg} = 0·68–0·70, with $X_{Mg} = Mg/(Mg + Fe^{2+})$] and plagioclase ($An_{78–89}$) with subordinate but ubiquitous orthopyroxene (X_{Mg} = 0·62–0·66, and Wo < 1%). Magnetite is the dominant oxide, whereas ilmenite appears sporadically.

The occurrence of layered igneous-looking gabbroic rocks that show transition to mafic migmatites over short distances provides evidence that the latter lithology is the partially melted equivalent of the former. Many of the mafic migmatites (e.g. specimens VFSJ11, 14, 16, 20, 25B) display both igneous and metamorphic textures at the thin-section scale, and have mineral compositions and assemblages similar to those of non-melted gabbroic rocks. Most of the mafic migmatites are hornblende gabbros and some of them are two-pyroxene gabbros showing medium-grained granoblastic textures. Mafic migmatites have a mineral preferred orientation fabric defined by the alignment of amphibole and plagioclase grains. Two-pyroxene mafic migmatites (e.g. VFSJ20) are characterized by the coexistence of plagioclase ($An_{70–77}$), Mg-hornblende to edenite amphibole (X_{Mg} = 0·64–0·67), clinopyroxene (X_{Mg} = 0·74–0·76, with Wo ~ 47%), orthopyroxene (X_{Mg} = 0·62–0·64), and magnetite.

Plagioclase- and quartz-rich leucotonalitic leucosomes within the darker mafic layers give the rock its migmatitic

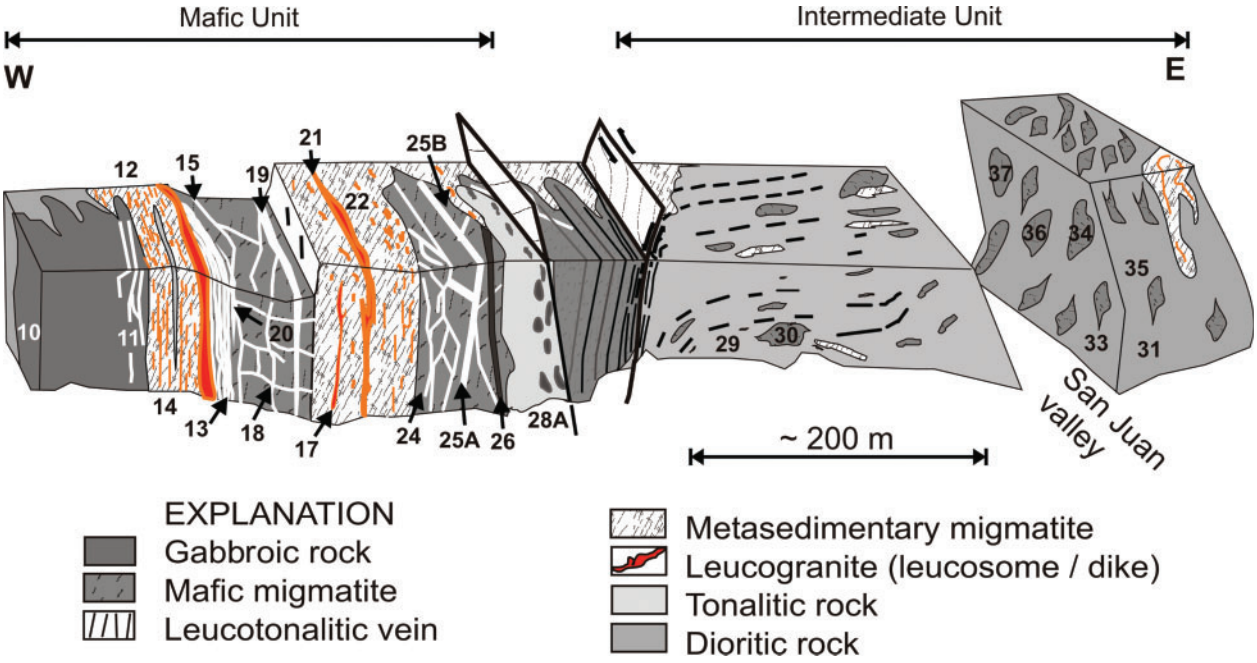

Fig. 3. Sketch cross-section through the contact between the mafic and intermediate units showing the field relationships and structural features (see Fig. 2 for location). Numbers show the sampling location of those specimens studied in detail. It should be noted also that numbers are equivalent to the full sample numbers presented in the figures and tables; for example, '10' is sample VFSJ10.

appearance (Fig. 4a). These white leucotonalites within the mafic migmatites are described in terms of increasing size as follows: layer-parallel, discordant leucosome trails (Fig. 4a), melt-filled boudin necks, small pools and veins (Fig. 4b), misaligned fragments of dykes (Fig. 4c; specimen VFSJ13), and tabular-shaped dykes forming patterns of fracturing and veining within the gabbroic or mafic rocks (Fig. 4d; specimens VFSJ15, 18, 19, 25A). Because there

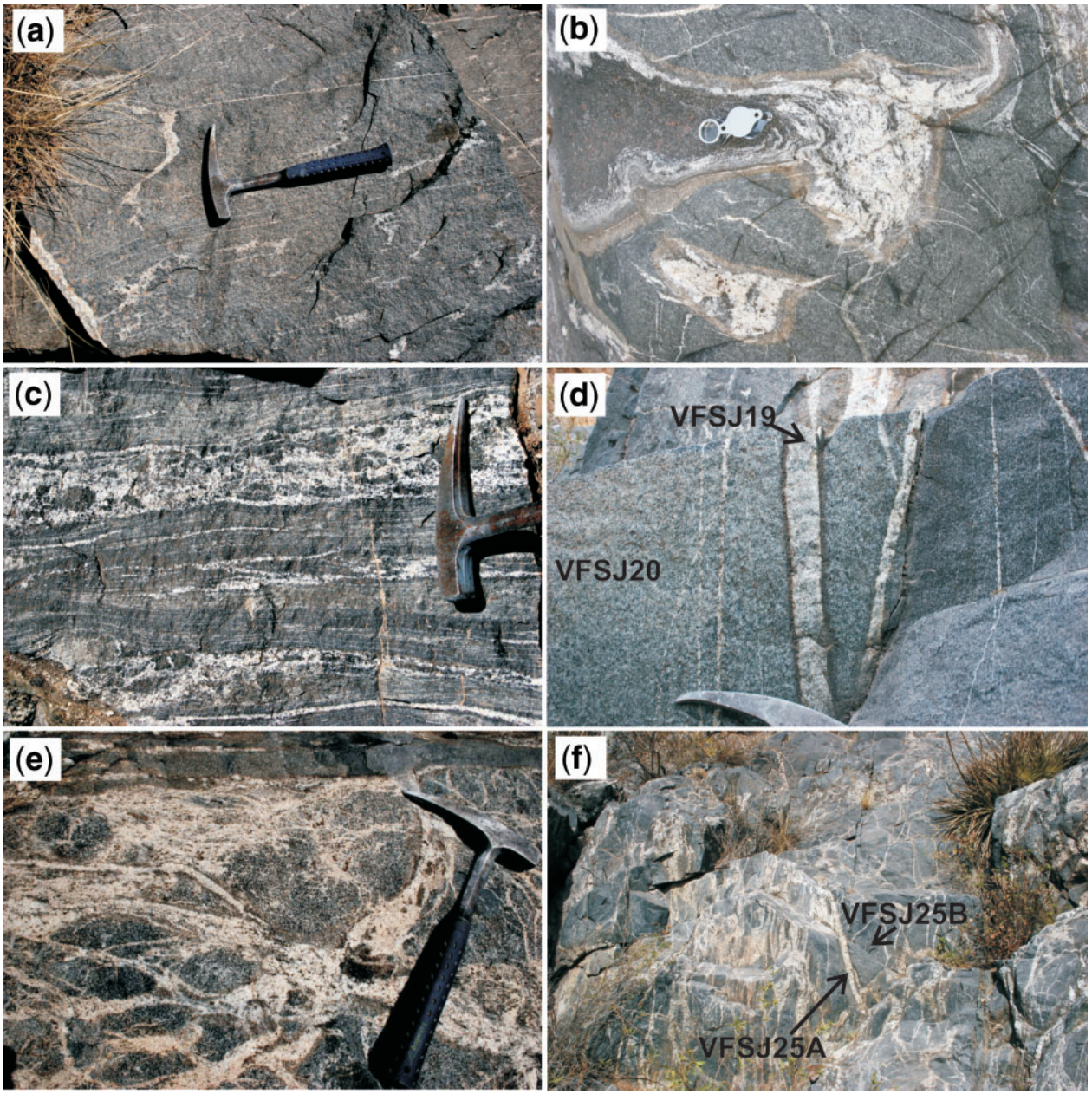

Fig. 4. (a) Leucotonalitic leucosomes in the mafic migmatites appearing as foliation-parallel veins and filling small boudin necks. Some leucotonalitic leucosomes fill asymmetric tension gashes, indicating that deformation was enhancing the movement of melts (e.g. Sawyer, 1991). (b) Mafic migmatites in which a leucotonalitic boudin neck is spatially related to a block of Bt- and Grt-rich metasedimentary rock (on which the lens is resting). The metasedimentary and gabbroic rocks were already interlayered when partial melting took place. (c) Leucotonalitic veins form an anastomosing system at centimetre-scale and an ill-defined tabular-shaped dyke at metre-scale. (d) Sharp-walled sill created by the coalescence of leucotonalitic veins in the mafic migmatite. The amphibole-rich band that appears along the wall of the sill was generated by reaction between the leucotonalitic magma and the mafic migmatite. (e) Photograph illustrating that the formation of large leucotonalitic pools within the mafic migmatites led to fragmentation of the mafic migmatite into centimetre-wide blocks. (f) Outcrop-scale photograph showing the 3-D distribution of the leucotonalitic veins (the field of view is around 5 m). In most cases the relative location of the photograph may be obtained by matching the sample numbers with those shown in Fig. 3.

exists a close spatial relationship between the metamorphic overprinting in the gabbroic rocks and the presence of leucotonalitic leucosomes, it is inferred that the mafic migmatites are the end result of two related processes: (1) *in situ* leucosome-forming partial melting of gabbroic protoliths; (2) mineral recrystallization in reaction zones formed between a system of leucotonalitic veins and/or dykes and the host gabbroic rocks. A somewhat simple distinction between the 'segregated' and 'vein' leucocratic component in migmatites permits the genetic implications of distinct leucotonalites to be distinguished (e.g. Sawyer, 1991). Whereas the segregated leucosomes reflect virtually *in situ* partial melting, the veins represent pathways that were used during transport of melts away from the site of first generation. Although we have distinguished leucotonalites forming both segregations and veins (see Fig. 4a and c), all the leucotonalitic rocks sampled in the field come from veins. The patterns of fracturing and veining show a 3-D stockwork lattice indicating that the rheological response of the gabbroic packages during the transference of tonalitic magmas was mainly brittle (Fig. 4f). Locally strain partitioning led to the development of high-strain belts where the behaviour of the rocks was dominantly ductile (Fig. 4b). Leucotonalitic veins form an interconnected network that is mainly developed within mafic migmatites but extends into tonalitic and dioritic bodies. Coalescence of leucotonalitic veins forms discrete tonalitic bodies (Fig. 4e).

Leucotonalitic veins comprise mostly plagioclase (45–62%) and quartz (20–50%). Variable combinations of other phases occurs in minor amounts, including hornblende, clinopyroxene, orthopyroxene, biotite, K-feldspar, epidote, sphene, magnetite, and pyrite. Plagioclase composition varies between calcic andesine (An_{39}) and sodic labradorite (An_{52}), but crystal zoning generally varies only over a narrow range ($An_{44–48}$). In some leucotonalitic veins (e.g. VFJS19), andesine grains show intragranular fractures filled by oligoclase ($An_{11–16}$), and in the same veins K-feldspar appears as small but discrete grains. Most leucotonalitic veins contain no ferromagnesian minerals. Hornblende and pyroxenes, when present in the leucotonalitic veins, are more abundant towards the outer parts and are thought to be disaggregated crystals from the hosting gabbroic or mafic rocks, rather than crystallized from the leucotonalitic magma; they commonly have a clinopyroxene-rich reaction zone adjacent to tonalitic veins. Clinopyroxene ($X_{Mg} = 0{\cdot}72–0{\cdot}76$, and Wo ~47%), which occurs locally in the gabbroic rocks, appears in large modal proportion between the veins and the host mafic migmatite.

The youngest mafic dykes cut across the already formed migmatitic fabric of the early crystallized gabbroic rocks, suggesting that the ascent and intrusion of the mafic melts spans a time longer than the melting event (Fig. 5a, and specimen VFSJ26). Late mafic dykes contain the most pristine fine-grained hypidiomorphic textures and consist of hornblende, plagioclase, magnetite, and minor clinopyroxene. Fine-grained mafic dykes consist of hornblende ($X_{Mg} = 0{\cdot}66–0{\cdot}69$) and plagioclase ($An_{74–85}$) with mineral compositions roughly similar to those of the layered hornblende gabbros, suggesting that the magma compositions feeding the gabbroic layers remained broadly constant through time.

Metasedimentary migmatite

Metasedimentary migmatites occur as wedge-shaped or linear packages intercalated among the gabbroic rocks (Figs 2 and 3). In most cases, the metasedimentary migmatites display stromatic morphology with millimetre- to centimetre-scale layers of alternating biotite-rich mesosomes and foliation-parallel quartzo-feldspathic leucosomes (Fig. 5b). The proportion of leucosome in the migmatites varies from nearly zero (VFSJ12) to around 40% by volume (VFSJ22). Metasedimentary migmatites consist of biotite, quartz, plagioclase, sillimanite and K-feldspar, with variable amounts of garnet and cordierite. All migmatites are foliated, with foliation defined by aligned biotite + sillimanite ± garnet. Within the metasedimentary migmatites, millimetre-wide leucosomes are interconnected with lens- and tabular-shaped centimetre-wide leucogranitic dykes (VFSJ17 and 21 and Fig. 5c). These leucogranitic dykes are considered to be an interconnected system of channelways through which anatectic melts moved (e.g. Sawyer, 1996). Centimetre-wide leucogranitic veins, sourced from the metasedimentary migmatite, intrude into the mafic migmatites (Fig. 5c). Significantly, the composition of those veins that cut across the contact between the metasedimentary migmatites and gabbroic rocks changes sharply from leucogranite to leucotonalite at the contact. On the other hand, metasedimentary migmatitic packages are locally cut by chilled mafic dykes and leucotonalitic veins (specimen VFSJ24).

Intermediate unit

Dioritic and tonalitic bodies

The boundary between the mafic and intermediate rocks units is gradational and occurs over a distance of few hundred metres (Figs 2 and 3). In the studied section, the complex interstratified lithological sequence of the mafic unit grades eastward (upward in the crustal section) to tonalitic and dioritic rocks (Fig. 3). Lens-shaped tonalitic bodies can be seen along the eastern border of the gabbroic zone, and their appearance marks the transition between mafic and intermediate rock units. These tonalitic bodies are few metres to tens of metres wide and flanked by metre-wide layers of mafic migmatites (specimens VFSJ28 and 29).

Within the intermediate unit, tonalites and diorites are coarse- to medium-grained, well foliated, and consist of plagioclase ($An_{47–62}$), quartz, hornblende, and biotite

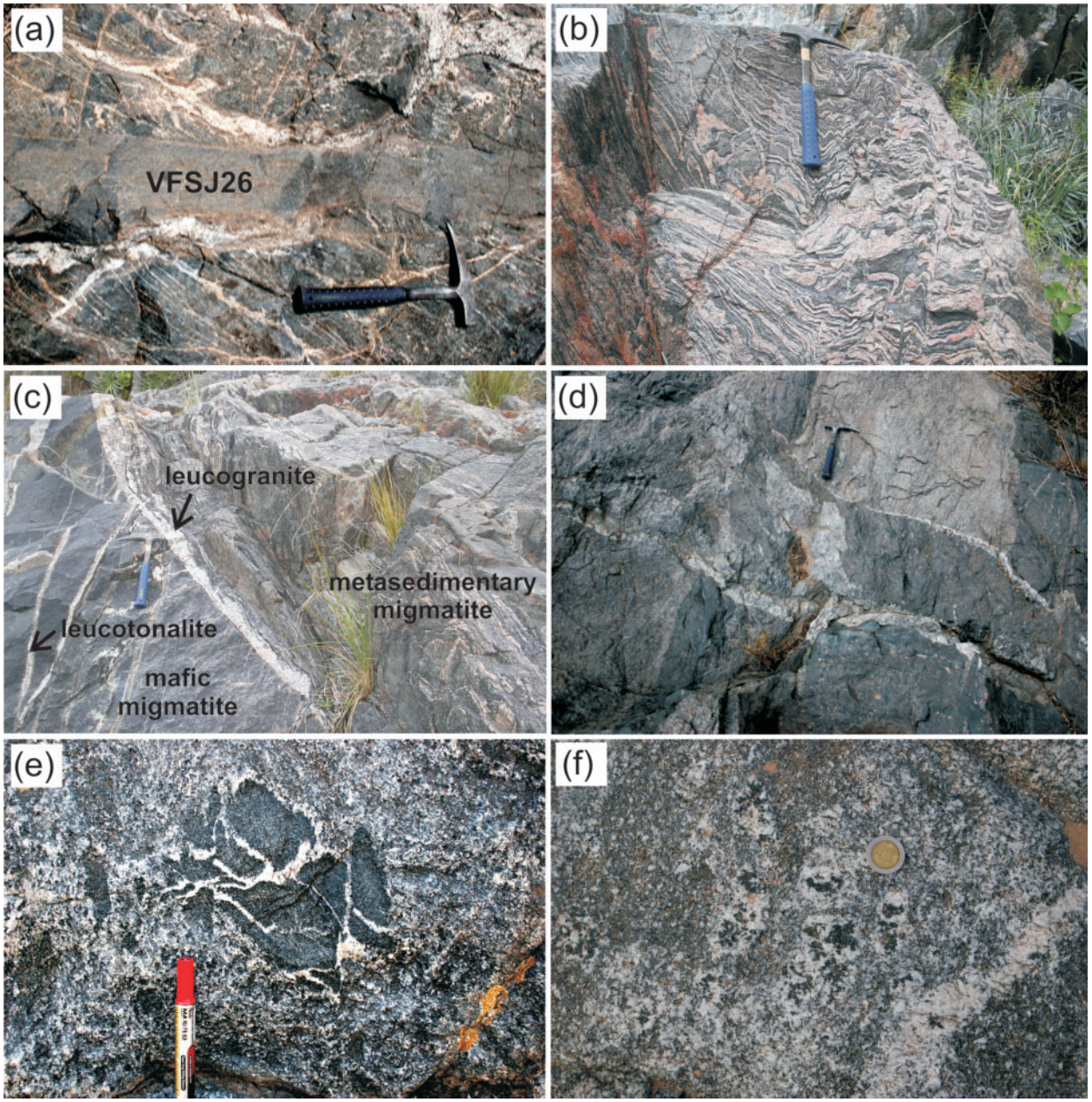

Fig. 5. (a) Fine-grained amphibole-gabbros appear as tabular-shaped sills and dykes intruding into and cutting across the already formed mafic migmatitic structure. (b) Metasedimentary stromatic migmatite defined by the alternation of leucogranitic leucosomes and granulite-facies paragneissic mesosomes. Melt-enriched and melt-depleted migmatitic layers in a single metasedimentary package suggest that the generation and redistribution of anatectic melts was heterogeneous on a metre-scale. (c) Sharp contact between metasedimentary (on the right side) and mafic migmatites. Leucogranitic dykes segregated from the metasedimentary migmatite are connected with leucotonalitic veins sourced from the mafic migmatite, indicating that metasedimentary and mafic migmatites underwent partial melting at the same time and under similar physical conditions (the field of view is around 2·5 m in width). (d) Blocky-shaped inclusion of gabbroic rocks in host diorite. (e) Rounded small gabbroic inclusions in host dioritic rocks, showing the occurrence of amphibole-enriched haloes surrounding the inclusion. (f) Hornblende clots surrounded by plagioclase-rich zones in diorite.

(VFSJ31 and 33, and VFSZ4A). The modal abundance of hornblende is higher in the diorites, whereas the biotite proportion is subordinate. Furthermore, the magnesium-number of coexisting hornblende and biotite is broadly equal (0·64–0·67, as measured in specimen VFSJ29). The typical foliation is defined by the subparallel alignment of hornblende, biotite, and plagioclase crystals. The absence of intragranular deformation suggests that the weak but

widespread foliation is mainly due to magmatic flow. The common observation of recrystallized quartz ribbons reflects overprinting by a sub-solidus tectonic foliation.

A typical feature of the tonalitic and dioritic bodies is the widespread occurrence of dark fine- to medium-grained amphibole-rich gabbroic fragments (Fig. 5d). Several specimens (VFSJ30, 34, 36, 37, and VFSZ4B) display all the modal, textural and size variations found in the gabbroic fragments (Table 1). The existence of centimetre-thick amphibole-enriched haloes surrounding the gabbroic fragments documents the assimilation of gabbroic rocks by the evolving tonalitic and/or dioritic magmas (Fig. 5e). As this assimilation process advanced, there was an increase in the relative proportion of dioritic and tonalitic rocks and a decrease in the amount of gabbroic inclusions. This resulted in the formation of lens-shaped gabbroic inclusions amounting to tens per cubic metre. At even a more advanced stage of assimilation is shown by the occurrence of clusters of incipiently resorbed amphibole phenocrysts (Fig. 5f). Another striking feature of the dioritic bodies is that the fine-grained gabbroic fragments (e.g. VFSJ36) are mafic migmatites containing leucotonalitic veins (specimen VFSJ35). These field relationships are taken to indicate that the growing tonalitic and dioritic magmatic bodies incorporated, and to some extent assimilated, previously formed mafic migmatites. Irregular-shaped fragments of metasedimentary migmatites are also present in the dioritic–tonalitic bodies. The local occurrence in the diorites and tonalites of pods with garnet-bearing and biotite-rich assemblages is inferred to reflect partly assimilated metasedimentary fragments. Importantly, tonalitic and dioritic rocks emplaced close to the boundary between the mafic and intermediate units contain partially assimilated fragments from all the lithologies that make up the upper part of the mafic unit.

GEOCHEMISTRY

Whole-rock major and trace element data were determined by X-ray fluorescence (XRF) and inductively coupled plasma mass spectrometry (ICP-MS), and are reported in Table 2. Sr and Nd isotopic data are presented in Table 3.

Analytical methods

The majority of the specimens taken for whole-rock chemical analyses consist of more than 2 kg of unaltered material. Leucogranitic dykes and leucotonalitic veins were separated from their adjoining mesosomes using a diamond saw. We were able to collect between 1 and 2 kg for the leucogranites and about 0·5 kg for the leucotonalitic veins. After crushing the whole sample, *c.* 500 g of homogeneous material was ground to a powder in a tungsten-carbide grinding bowl. The container was always pre-contaminated with the sample about to be pulverized.

Major elements and selected trace elements (Ba, Rb, Sr, and Zr) were determined by XRF at the University of Huelva, Spain. Loss on ignition (LOI) was determined separately. All XRF measurements were carried out using a wavelength-dispersive XRF S4 Pioneer (Bruker AXS, Karlsruhe, Germany). Both major and trace elements were determined on glass beads, which were made by fusing 1 g ignited rock powder with 10 g LiB_4O_7 plus five drops of LiI at 20%. International standards were used in the calibration.

Most trace elements were determined by ICP-MS using an HP4500® housed at the University of Huelva, Spain. A 100 mg fraction of powder was digested for 48 h in a solution consisting of HF (8 ml) and HNO_3 (3 ml) in PTFE SAVILLEX® vessels at ~90°C (on hot plates). After evaporation to dryness each sample was re-dissolved in HNO_3 (ml) and HCl (ml) for 24 h. Subsequently, after drying, the sample was diluted in 100 ml of 3% HCl solution for 24 h. Finally, after evaporation, each sample was diluted in 100 ml of 2% HNO_3. Three multi-elemental solutions Spec® 1 (rare earth elements; REE), Spec® 2 (alkalis, earth alkalis, and metals) and Spec® 4 (Nb) were used to construct an external calibration curve. The accuracy and the reproducibility of the reported values, as determined on the international standards SARM1 and SARM4, is in general between 5 and 10% relative.

The isotopic ratios of $^{87}Sr/^{86}Sr$ and $^{143}Nd/^{144}Nd$, and the trace element concentrations of Rb, Sr, Sm, and Nd were measured by thermal ionization mass spectrometry on whole-rock samples. Rock powders were put in large Savillex vials and dissolved in mixtures of hot concentrated HF–HNO_3 or alternatively, mixtures of cold concentrated HF–$HClO_4$. The dissolved samples were spiked with the Caltech Rb, Sr, and mixed Sm–Nd spikes (Wasserburg *et al.*, 1981; Ducea & Saleeby, 1998) after dissolution. Rb, Sr, and the bulk of the REE were separated in cation columns containing AG50W-X4 resin, using 1N–4N HCl. Separation of Sm and Nd was achieved in anion columns containing LN Spec resin, using 0·1N–2·5N HCl. Rb was loaded onto single Re filaments using silica gel and H_3PO_4. Sr was loaded onto single Ta filaments with Ta_2O_5 powder. Sm and Nd were loaded onto single Re filaments using platinized carbon, and resin beads, respectively. Mass spectrometric analyses were carried out at the University of Arizona on an automated VG Sector multicollector instrument fitted with adjustable Faraday collectors and a Daly photomultiplier (Ducea & Saleeby, 1998). Concentrations of Rb, Sr, Sm, Nd were determined by isotope dilution, with isotopic compositions determined on the same spiked runs. An off-line program was used for the isotope dilution calculations. Typical runs consisted of acquisition of 100 isotopic ratios. The mean result of 10 analyses of the standard NRbAAA performed during the course of this study is

Table 1: Summary of petrographic observations

Unit and group	Rock type	Mineralogy	Observations
Mafic unit			
Gabbroic rocks			
VFSJ10	two-Px Amph gabbro	Hbl–Pl–Opx–Cpx–Mag–Ap	Hypidiomorphic inequigranular. Banding Pl-rich/Amph-rich bands. Relic subophitic
Mafic migmatites			
VFSJ11		Hbl–Pl–Opx–Bt–Mag–Qtz	
VFSJ14		Pl–Hbl–Qtz–Mag–Cum	
VFSJ16	Amph gabbro	Pl–Cpx–Hbl–Ap–Mag	Hypidiomorphic inequigranular.
VFSJ20	Px Amph gabbro	Cpx–Opx–Pl–Hbl–Mag	Nematoblastic. Relict hypidiomorphic texture.
VFSJ25B	two-Px Amph gabbro	Pl–Hbl–Cpx–Qtz–Chl–Ap	Locally pseudopolygonal recrystallization
Mafic dyke			
VFSJ26	Amph gabbro	Hbl–Pl–Opx–Mag–Ap	Hypidiomorphic equigranular. Mineral elongation parallel to Amph alignment
Leucotonalitic veins			
VFSJ13			
VFSJ15			Hypidiomorphic inequigranular coarse-
VFSJ18	Bt leucotonalite	Pl–Qtz–Bt–Ep–Mag–Chl	grained, or xenomorphic granular. Reaction
VFSJ19	Cpx Amph tonalite	Pl–Qtz–Hbl–Cpx–Mag–Ap	zone transitional from Pl–Op- to Cpx–Pl-rich
VFSJ24	Bt Amph tonalite	Pl–Qtz–Kfs–Bt–Mag–Ap–Spn	layer. Locally, pseudopolygonal with Cpx +
VFSJ25A	Opx Bt tonalite	Pl–Qtz–Opx–Bt–Mag–Zrn	Amph + Pl in textural equilibrium
Metasedimentary migmatites within the mafic unit			
VFSJ12			Compositional layering Qtz-rich/Bt-rich
VFSJ22	paragneissic migmatite	Qtz–Pl–Bt–Kfs–Grt–Sil–Crd–Mag	bands. Textural reworking Qtz–Pl–Crd appear as microlithons flanked by discontinuous band of Bt + Qtz + Op
Leucogranites			
VFSJ17			Xenoblastic coarse-grained. Textural
VFSJ21	Bt ± Ms ± Grt leucogranite	Qtz–Kfs–Pl–Bt–Ms–Grt	reworking leucocratic layers (Qtz–Kfs–Pl) surrounded by sutured matrix (Qtz)
Intermediate unit			
Tonalitic rocks			
VFSJ28	Bt tonalite	Pl–Qtz–Bt–Mag–Zrn	Hypidiomorphic inequigranular. Textural
VFSJ29	Bt tonalite	Pl–Qtz–Hbl–Bt–Mag–Ap–Zrn	reworking, dynamic reduction of Qtz size. Mineral elongation parallel to Bt lath alignment
Dioritic rocks			
VFSJ31		Pl–Qtz–Hbl–Bt–Mag–Ms	
VFSJ33		Pl–Hbl–Bt–Cpx–Qtz–Ap	Hypidiomorphic inequigranular medium-
VFSZ4A	Amph diorite	Pl–Qtz–Hbl–Mag	grained. Pl-phyric. Mineral preferred
VFSJ35	Bt leucotonalite	Pl–Qtz–Bt–Ap–Zrn–Mag	orientation
Gabbroic inclusions within dioritic and tonalitic rocks			
VFSJ30		Hbl–Pl–Opx–Cpx–Mag	
VFSJ34		Pl–Hbl–Opx–Bt–Mag–Ap	Hypidiomorphic granular. Medium to coarse-
VFSJ36		Cpx–Opx–Pl–Hbl–Bt–Zrn	grained. Pseudopolygonal recrystallization.
VFSJ37	two-Px Amph gabbro	Pl–Hbl–Opx–Qtz–Mag–Bt	Idioblastic. Locally cumulate texture to
VFSZ4B	Px Amph gabbro	Pl–Hbl–Opx–Bt–Mag–Ap	granoblastic

Table 2: Whole-rock major element (wt %) and trace element (ppm) composition

	Gabbro	Mafic migmatite					Chilled dyke	Metasedimentary migmatite		Leucogranite		Leucotonalitic vein		
	VFSJ10	VFSJ11	VFSJ14	VFSJ16	VFSJ20	VFSJ25B	VFSJ26	VFSJ12	VFSJ22	VFSJ17	VFSJ21	VFSJ13	VFSJ15	VFSJ18
SiO_2	46·73	51·90	51·26	51·36	51·58	50·89	44·54	55·82	69·15	73·82	74·95	62·47	66·84	68·80
TiO_2	0·75	0·52	0·92	0·97	0·67	0·71	1·07	1·32	0·79	0·11	0·08	0·86	0·20	0·41
Al_2O_3	16·20	16·00	14·46	13·33	16·59	15·23	17·75	19·52	13·76	13·93	14·99	17·14	18·10	15·87
Fe_2O_3	12·54	9·80	11·11	12·01	9·08	9·68	14·62	12·33	7·58	1·66	0·57	5·19	2·76	3·77
MnO	0·21	0·15	0·19	0·20	0·16	0·17	0·25	0·27	0·14	0·03	0·02	0·08	0·04	0·06
MgO	8·44	8·07	7·89	8·34	7·59	8·31	7·53	5·43	2·62	0·44	0·21	3·12	1·10	1·61
CaO	12·05	10·92	11·26	11·16	12·23	12·05	11·44	1·41	1·21	1·38	1·39	4·61	7·52	4·71
Na_2O	1·06	0·93	1·21	1·84	1·70	1·45	1·21	1·54	1·93	2·43	2·93	3·18	3·27	3·19
K_2O	0·51	0·73	0·57	0·59	0·50	0·65	0·47	1·78	3·55	4·69	6·29	2·20	0·40	1·40
P_2O_5	0·05	0·01	0·09	0·08	0·06	0·07	0·13	0·02	0·04	0·05	0·09	0·18	0·09	0·10
LOI	1·38	1·38	1·20	0·60	0·59	0·85	1·17	1·27	0·92	1·20	0·41	1·15	0·40	0·68
Total	99·92	100·41	100·15	100·48	100·74	100·06	100·18	100·70	101·69	99·75	101·93	100·17	100·73	100·60
Rb	12	35	7	5	3	8	6	79	74	73	77	90	6	60
Sr	140	113	97	105	110	109	151	110	128	261	246	193	160	165
Zr	63	n.a.	241	n.a.	n.a.	n.a.	42	271	148	103	96	33	n.a.	n.a.
Ba	86	125	74	39	60	74	67	301	539	1017	1833	373	52	233
Sc	55·9	44·1	46·9	49·8	45·2	47·4	50·2	26·3	18·1	1·7	0·9	17·7	10·6	9·9
V	349·0	319·2	212·8	335·1	170·0	176·5	388·1	156·3	81·0	18·1	4·1	108·3	71·0	92·5
Cr	227·4	269·6	267·4	120·2	187·2	469·8	79·9	118·3	73·7	16·7	2·1	34·5	69·6	7·7
Co	57·3	57·5	56·2	60·4	52·4	52·0	55·9	62·2	77·3	115·6	72·2	48·6	72·5	64·8
Ni	52·7	59·2	94·7	80·1	96·8	105·5	50·7	68·1	51·0	5·1	3·9	29·1	14·7	14·0
Cu	110·5	120·2	140·1	125·7	79·7	90·5	225·4	1·9	2·4	0·4	3·4	80·7	2·8	36·0
Zn	77·7	54·2	69·5	76·5	56·7	60·6	94·8	143·6	86·7	8·2	10·1	62·9	28·5	36·7
Y	16·7	16·1	22·5	23·2	17·7	20·4	20·8	9·9	12·7	6·2	6·3	18·2	16·0	10·5
Nb	3·4	5·6	3·6	3·6	3·4	3·7	3·0	18·7	11·8	1·7	1·1	14·8	2·7	8·6
Cs	0·5	0·7	0·2	0·7	0·1	0·3	0·2	2·5	1·0	1·2	0·5	1·5	2·6	1·2
La	8·38	20·15	6·00	6·83	5·88	7·91	8·05	44·82	46·62	20·64	27·83	50·07	9·17	17·20
Ce	20·09	40·60	13·49	15·30	13·88	17·91	20·36	78·30	86·82	35·63	48·29	84·93	17·36	30·93
Pr	2·62	4·84	1·78	2·00	1·81	2·43	2·97	9·79	12·18	3·99	5·73	10·88	1·96	3·27
Nd	10·94	17·86	8·09	8·72	7·65	8·81	12·92	34·86	31·53	14·69	14·68	38·94	7·91	11·56
Sm	2·79	3·59	2·34	2·54	2·13	2·40	3·46	5·97	5·69	2·12	2·51	6·76	2·07	2·30
Eu	0·82	0·70	0·95	0·98	0·79	0·86	1·21	1·30	1·68	2·43	2·69	1·74	0·65	1·11
Gd	3·11	3·43	3·34	3·51	2·74	3·21	3·90	4·92	6·39	1·79	2·68	6·04	2·44	2·33
Tb	0·56	0·57	0·64	0·66	0·51	0·58	0·67	0·61	0·82	0·27	0·35	0·83	0·46	0·38
Dy	3·11	3·02	3·93	4·08	3·21	3·69	3·96	2·48	3·52	1·42	1·54	3·93	2·72	2·08
Ho	0·79	0·73	1·03	1·07	0·86	0·98	1·03	0·47	0·65	0·27	0·29	0·87	0·70	0·48
Er	1·90	1·73	2·64	2·72	2·16	2·45	2·57	0·85	1·10	0·60	0·55	1·81	1·75	1·06
Tm	0·36	0·31	0·49	0·49	0·34	0·38	0·38	0·11	0·10	0·09	0·06	0·25	0·32	0·17
Yb	1·68	1·46	2·47	2·52	1·98	2·30	2·25	0·42	0·42	0·50	0·26	1·04	1·54	0·77
Lu	0·31	0·26	0·46	0·47	0·32	0·36	0·35	0·07	0·05	0·08	0·03	0·17	0·26	0·13
Pb	11·60	16·90	8·80	14·50	8·70	10·30	13·20	21·40	34·70	19·30	29·30	19·60	20·10	19·60
Th	2·74	9·18	1·55	1·02	1·35	1·23	0·98	18·55	22·10	2·50	8·97	18·52	0·57	4·14

(continued)

Table 2: Continued

	Leucotonalitic veins					Tonalitic rock			Dioritic rock			Gabbroic inclusion in dioritic rocks		
	VFSJ19	VFSJ24	VFSJ25A	SJ28	SJ29	VFSJ31	VFSJ33	VFSZ4A	VFSJ35	VFSJ30	VFSJ34	VFSJ36	VFSJ37	VFSZ4B
SiO_2	75·34	75·36	68·20	56·02	59·78	54·54	54·64	54·39	68·99	48·89	45·21	44·96	44·14	46·77
TiO_2	0·09	0·30	0·05	0·94	1·00	0·95	0·93	0·95	0·53	0·49	0·77	1·62	1·66	1·00
Al_2O_3	14·56	13·66	17·75	19·45	17·21	17·79	18·09	17·98	14·91	10·58	18·26	16·65	16·95	16·13
Fe_2O_3	0·70	2·02	0·64	8·40	7·95	9·65	9·57	9·69	3·72	10·06	13·67	18·11	18·67	13·88
MnO	0·01	0·06	0·04	0·09	0·13	0·15	0·14	0·15	0·05	0·26	0·23	0·24	0·26	0·21
MgO	0·43	0·63	0·38	3·05	3·11	4·22	4·38	4·46	2·40	14·16	7·96	5·59	5·86	7·41
CaO	4·70	2·73	6·48	5·50	6·14	7·47	7·90	8·16	5·91	12·10	10·91	10·78	11·00	10·97
Na_2O	3·06	3·84	3·95	3·04	2·52	2·66	2·44	2·65	1·72	0·96	1·65	1·36	1·44	1·50
K_2O	0·47	0·74	0·82	2·45	1·88	1·55	1·44	0·96	1·11	0·95	0·71	0·42	0·36	0·80
P_2O_5	0·06	0·10	0·82	0·03	0·20	0·20	0·18	0·17	0·15	0·03	0·07	0·06	0·02	0·02
LOI	0·60	0·71	0·87	1·12	0·49	0·96	0·87	0·64	0·98	1·97	0·84	0·14	0·28	1·27
Total	100·01	100·15	100·01	100·09	100·40	100·15	100·57	100·19	100·46	100·45	100·28	99·94	100·64	99·96
Rb	16	17	18	99	79	52	51	27	49	20	16	6	3	16
Sr	153	189	178	209	187	186	188	208	177	72	184	162	168	208
Zr	n.a.	80	n.a.	178	216	139	116	112	125	n.a.	n.a.	n.a.	n.a.	n.a.
Ba	116	84	134	480	364	338	275	402	210	116	99	70	58	203
Sc	2·8	4·9	3·1	20·7	21·4	41·4	39·5	36·2	7·8	56·0	41·4	54·2	54·3	59·2
V	14·6	32·6	4·2	126·3	143·9	172·4	174·3	177·9	89·8	164·7	335·7	469·8	469·2	415·9
Cr	5·7	8·7	7·8	17·3	36·4	39·9	44·6	48·9	24·3	1374·8	29·4	25·1	30·8	20·1
Co	71·5	75·7	87·0	45·6	55·2	44·8	53·0	46·7	63·6	51·9	59·3	65·9	61·5	56·9
Ni	8·1	12·8	6·1	18·7	23·7	23·6	26·2	27·2	20·0	165·0	50·7	20·6	22·6	34·2
Cu	22·6	3·0	6·3	65·8	52·4	78·2	50·5	52·8	98·2	56·2	145·8	156·2	159·9	114·6
Zn	19·6	30·5	13·7	89·7	89·2	84·3	83·7	92·0	40·3	76·0	89·8	127·8	128·6	90·5
Y	10·3	25·5	60·1	4·5	22·5	43·5	36·0	42·9	4·3	28·9	14·2	21·0	18·2	30·8
Nb	4·2	6·6	1·5	16·9	10·2	10·8	11·1	8·4	6·3	4·8	2·7	6·0	3·8	4·8
Cs	0·2	0·8	0·6	1·4	1·6	0·8	0·7	0·4	0·7	0·2	0·2	0·2	0·1	0·3
La	20·08	72·54	28·13	35·61	15·73	19·91	19·50	17·96	11·00	13·30	10·45	10·97	9·85	9·83
Ce	35·61	213·30	62·00	63·00	33·82	48·81	46·77	46·65	20·27	38·59	24·01	24·92	21·40	28·59
Pr	3·78	21·50	9·49	8·02	4·73	8·24	7·58	8·15	2·21	6·09	3·05	3·36	2·78	4·75
Nd	12·28	74·82	29·25	27·28	15·65	30·66	25·20	32·06	7·72	24·34	11·35	13·41	11·28	21·62
Sm	2·41	14·37	8·55	4·12	3·78	7·48	6·09	8·09	1·28	5·73	2·54	3·44	2·91	5·87
Eu	1·02	2·41	1·85	1·61	1·36	1·90	1·62	2·03	0·69	1·32	1·06	1·10	0·92	1·23
Gd	2·35	11·84	12·53	2·95	4·71	9·65	7·56	9·32	1·19	5·59	2·68	3·83	3·23	6·20
Tb	0·37	1·59	2·42	0·30	0·78	1·61	1·26	1·54	0·16	0·96	0·44	0·69	0·58	1·04
Dy	1·93	7·05	13·89	1·12	4·49	9·34	7·31	8·86	0·85	5·56	2·60	4·09	3·59	6·15
Ho	0·44	1·29	3·30	0·20	1·12	2·33	1·84	2·20	0·19	1·40	0·66	1·05	0·89	1·54
Er	0·99	2·22	7·23	0·41	2·67	5·70	4·50	5·45	0·47	3·54	1·69	2·66	2·26	3·79
Tm	0·16	0·21	0·95	0·05	0·40	0·83	0·68	0·82	0·06	0·55	0·26	0·40	0·33	0·56
Yb	0·66	0·77	4·77	0·24	2·15	4·64	3·87	4·59	0·36	3·32	1·60	2·36	2·01	3·11
Lu	0·10	0·09	0·63	0·04	0·32	0·66	0·57	0·68	0·05	0·52	0·25	0·36	0·31	0·47
Pb	17·50	22·80	32·10	22·50	23·80	13·70	20·30	12·90	18·10	18·10	12·40	16·60	18·90	10·60
Th	6·41	33·22	9·43	12·60	0·95	0·75	0·55	0·44	0·33	1·25	0·63	1·10	1·41	1·27

Fe_2O_3 is total Fe; n.a. indicates that the analytical data are not accurate enough to be used.

Table 3: Isotope and trace element data

Rock type	Sample	Rb (ppm)	Sr (ppm)	$^{87}Rb/^{86}Sr$	$^{87}Sr/^{86}Sr$	$^{87}Sr/^{86}Sr$ [485 Ma]	Sm (ppm)	Nd (ppm)	$^{147}Sm/^{144}Nd$	$^{143}Nd/^{144}Nd$	$^{143}Nd/^{144}Nd$ [485 Ma]	ε_{Nd} [485 Ma]
Gabbroic rock	VFSJ10	12·31	140·23	0·1274	0·707135	0·706257	2·79	10·94	0·1765	0·512584	0·512024	+0·25
Mafic migmatite	VFSJ11	34·88	113·33	0·8857	0·716446	0·710346	3·59	17·86	0·1215	0·512101	0·511716	−5·77
Mafic migmatite	VFSJ16	4·95	105·03	0·1355	0·706167	0·705234	2·54	8·72	0·1760	0·512684	0·512126	+2·24
Mafic migmatite	VFSJ25B	7·74	108·81	0·2046	0·707749	0·706340	2·40	8·81	0·1646	0·512485	0·511963	−0·94
Metasediment	VFSJ22	73·65	127·62	1·6627	0·726894	0·715443	5·69	31·53	0·1090	0·512014	0·511668	−6·70
Leucogranite	VFSJ21	76·87	245·89	0·9001	0·721126	0·714927	2·51	14·68	0·1033	0·512021	0·511693	−6·21
Leucotonalitic vein	VFSJ15	6·33	159·55	0·1140	0·708316	0·707531	2·07	7·91	0·1584	0·512378	0·511876	−2·65
Leucotonalitic vein	VFSJ19	15·69	152·69	0·2834	0·713092	0·711140	2·41	12·28	0·1186	0·512121	0·511745	−5·21
Leucotonalitic vein	VFSJ25A	18·36	177·51	0·2976	0·714656	0·712606	8·55	29·25	0·1767	0·512245	0·511684	−6·39
Tonalitic rock	VFSJ28	98·84	209·11	1·3609	0·721206	0·711833	4·12	27·28	0·0913	0·512020	0·511730	−5·49
Tonalitic rock	VFSJ29	78·56	186·77	1·2110	0·719992	0·711652	3·78	15·65	0·1458	0·512190	0·511728	−5·54
Dioritic rock	VFSJ31	52·48	186·49	0·8100	0·714670	0·709092	7·48	30·66	0·1475	0·512256	0·511788	−4·36
Dioritic rock	VFSJ33	50·87	187·57	0·7805	0·716044	0·710668	6·09	25·20	0·1461	0·512209	0·511746	−5·19
Dioritic rock	VFSZ4A	27·03	208·36	0·3732	0·713478	0·710908	8·09	32·06	0·1525	0·512226	0·511742	−5·25

ε_{Nd} values are calculated as deviations from a chondritic uniform reservoir in parts per 10^4, using present-day values of $^{143}Nd/^{144}Nd = 0{\cdot}512635$ and $^{147}Sm/^{144}Nd = 0{\cdot}1966$ (Wasserburg *et al.*, 1981; Faure, 1986). Ages of rocks are from an average of the Famatinian plutonism (485 Ma) reported by Pankhurst *et al.* (1998, 2000) and Stair *et al.* (2007).

$^{85}Rb/^{87}Rb = 2{\cdot}61199 \pm 20$. Ten analyses of standard Sr987 yielded mean ratios of $^{87}Sr/^{86}Sr = 0{\cdot}710285 \pm 7$ and $^{84}Sr/^{86}Sr = 0{\cdot}056316 \pm 12$. The mean results of five analyses of the standard nSmβ performed during the course of this study are $^{148}Sm/^{147}Sm = 0{\cdot}74880 \pm 21$ and $^{148}Sm/^{152}Sm = 0{\cdot}42110 \pm 6$. Ten measurements of the LaJolla Nd standard were performed during the course of this study. The standard runs yielded the following isotopic ratios: $^{142}Nd/^{144}Nd = 1{\cdot}14184 \pm 2$, $^{143}Nd/^{144}Nd = 0{\cdot}511853 \pm 2$, $^{145}Nd/^{144}Nd = 0{\cdot}348390 \pm 2$, and $^{150}Nd/^{144}Nd = 0{\cdot}23638 \pm 2$. The Sr isotopic ratios of standards and samples were normalized to $^{86}Sr/^{88}Sr = 0{\cdot}1194$, whereas the Nd isotopic ratios were normalized to $^{146}Nd/^{144}Nd = 0{\cdot}7219$. The estimated analytical $\pm 2\sigma$ uncertainties for samples analyzed in this study are $^{87}Rb/^{86}Sr = 0{\cdot}35\%$, $^{87}Sr/^{86}Sr = 0{\cdot}0014\%$, $^{147}Sm/^{144}Nd = 0{\cdot}4\%$ and $^{143}Nd/^{144}Nd = 0{\cdot}0012\%$. Procedural blanks averaged from five determinations were 10 pg Rb, 150 pg Sr, 2·7 pg Sm, and 5·5 pg Nd.

Major element variations

Within the study area mafic rocks, distinguished by having $SiO_2 < 52$ wt %, may be divided into high Mg-number (>58) and low Mg-number (<54) groups [where Mg-number = $100MgO/(MgO + FeO^*)$, molar]. Gabbroic rocks and mafic migmatitic mesosomes make up the high Mg-number group, whereas the chilled mafic dyke and all but one gabbroic inclusion in the dioritic or tonalitic bodies belong to the low Mg-number group (Fig. 6a). The low Mg-number of the chilled mafic dyke is due to its normal MgO (*c.* 7·5 wt %) but high $Fe_2O_3^*$ content that reflects the large modal proportion of magnetite. In contrast, a combination of low MgO and moderate to high $Fe_2O_3^*$ contents accounts for the low Mg-number of the gabbroic inclusions within the dioritic bodies. Furthermore, the gabbroic inclusions have similar Mg-number but higher MgO abundances compared with their hosting tonalitic and dioritic rocks (Fig. 6a). Irrespective of their Mg-number the gabbroic rocks and mafic migmatites from the mafic units and the gabbroic fragments included in diorites are subalkaline (Fig. 6b), strongly calcic (Fig. 6c) with medium K_2O contents (Fig. 6d), and metaluminous (Fig. 6e). It follows that all these mafic rocks are similar in terms of their major element chemical signature.

Mafic migmatites were sampled to collect the mesosomes, which are those parts of the migmatite found between the leucotonalitic veins; however, all the sampled mafic migmatites contain millimetre-wide layer-parallel segregated leucosomes. Compared with the gabbroic rocks, the mafic migmatites have higher SiO_2, K_2O and total alkalis contents (Fig. 6b and d, respectively). As separated from the mafic migmatites, the leucotonalitic veins have a wide range of SiO_2 contents between 62 and 75 wt %. Collectively, these leucotonalitic veins show a compositional trend of decreasing MgO, FeO^*, CaO and K_2O with increasing SiO_2. All leucotonalitic veins are

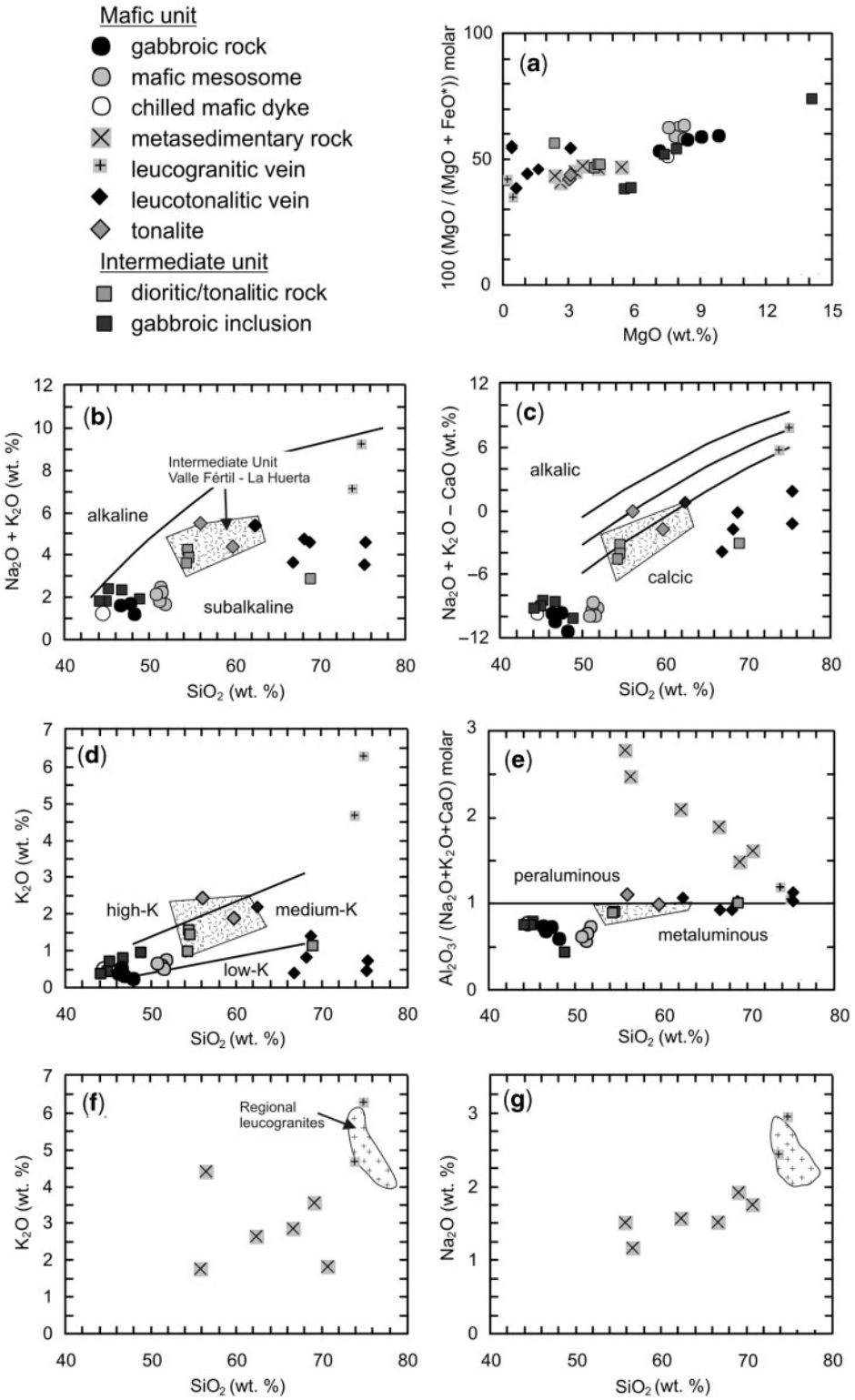

Fig. 6. Major element variations in the igneous, migmatitic and metasedimentary rocks. (a) Mg-number vs MgO. (b–e) Major element differentiation indices vs SiO_2 (wt %). In (b) and (d) the field boundaries are after Le Maitre *et al.* (1989). In (c) the field boundaries are from Frost *et al.* (2001). The compositional field of the intermediate unit from the Sierras Valle Fértil–La Huerta is from Otamendi *et al.* (2009). (f, g) K_2O and Na_2O vs SiO_2 wt % for the metasedimentary rocks and the anatectic leucogranites. For comparison, also shown is the compositional field of the leucogranites on a regional scale. Data for four metasedimentary migmatites and three gabbroic rocks included in the variation diagrams are from Otamendi *et al.* (2009).

strongly enriched in SiO_2 and Na_2O, but depleted in MgO, FeO, CaO and TiO_2 relative to their hosting mafic migmatites.

The most conspicuous compositional feature of the metasedimentary migmatites is a smooth negative correlation between alumina saturation index and SiO_2 abundance (Fig. 6e). This compositional trend most probably results from initial variations in the mineral mode of the protoliths, rather than from metamorphism or anatexis (Sawyer, 1987). The K_2O vs SiO_2 variation diagram for the metasedimentary migmatites is characterized by considerable scatter, without a definite compositional trend (Fig. 6f). In contrast, the other major alkaline oxide (Na_2O) plotted against SiO_2 displays a flat and smooth variation trend (Fig. 6g). Compared with the metasedimentary migmatites, the leucogranitic veins are strongly enriched in K_2O and slightly enriched in Na_2O (Fig. 6f and g), but depleted in Al_2O_3 and CaO (not shown).

Tonalitic and dioritic rocks differ from leucotonalitic veins in having less SiO_2 and Na_2O but more MgO and FeO*. Significantly, however, the tonalitic and dioritic rocks have total alkalis and CaO contents, Mg-number, and alumina saturation indices in the same range as the leucotonalitic veins (Fig. 6a–e). Thus, the leucotonalitic veins and tonalitic–dioritic rocks cannot be linked by closed-system fractional crystallization. This is because a K-absent ferromagnesian mineral would need to have crystallized to drive the differentiation trend recorded by the major elements; however, the leucotonalitic veins are characteristically leucocratic, even though they contain subordinate hornblende and pyroxene grains. The composition of the studied tonalitic and dioritic rocks shares similarities with other intermediate igneous rocks in the Sierras Valle Fértil–La Huerta area (Fig. 6b–e). Furthermore, over the range of most major elements, it is possible to recognize the chemical signature of the tonalitic and dioritic rocks, as they are all subalkaline, calcic or calc-alkaline, and weakly metaluminous rocks (Figs 6b–e). Overall, these major element characteristics resemble in many respects the compositional features of plutonic rocks found in most Cordilleran batholiths (e.g. Frost *et al.*, 2001).

Rare earth element variations

The mafic migmatites, the gabbroic rocks, and the mafic dyke have similar chondrite-normalized (REE_N) patterns, with the exception of mafic migmatite VFSJ11 (Fig. 7a). These rocks show no to minor negative Eu anomalies ($=Eu_N/Eu^*_N < 0{\cdot}85$, where $Eu^*_N = \sqrt{Sm_N.Gd_N}$) and little difference between light, middle and heavy REE (LREE, MREE and HREE)-normalized abundances ($La_N/Yb_N < 3$; $Gd_N/Yb_N = 1{\cdot}4$).

The leucotonalitic veins have different REE patterns (Fig. 7b). Two of the leucotonalites (VFSJ18 and 19) display similar REE patterns with high LREE to HREE ratios ($La_N/Yb_N = 15$–21) and positive Eu anomalies ($Eu_N/Eu^*_N > 1{\cdot}3$). All but one (VFSJ25a) of the leucotonalitic veins have low HREE contents with Yb_N lower than seven times chondritic concentration and high Gd_N/Yb_N ratios, ranging from 1·5 to 13·5.

The tonalitic rocks in contact with the mafic unit (tonalite samples SJVF28 and SJVF29) have distinctive REE patterns. One of the tonalites (VFSJ28) has an REE pattern with a very high La_N/Yb_N ratio and a positive Eu anomaly, resembling in many respects the REE pattern of the two leucotonalitic veins that have positive Eu anomalies (Fig. 7b). Relative to the tonalites, the dioritic rocks have higher total REE contents (ΣREE), lower La_N/Yb_N ratios (<3·5), and larger negative Eu anomalies ($Eu_N/Eu^*_N < 0{\cdot}66$) but with higher Eu abundances (Fig. 7d). Taken together, these differences in the REE contents make it unlikely that the tonalitic rocks were generated by closed-system crystallization from the dioritic rocks. The gabbroic inclusions in the diorites plot between those of the mafic migmatites and the dioritic bodies (Fig. 7a and d). A leucotonalitic vein (SJVF35) and its host gabbroic inclusion (SJVF36), both included in a diorite, have the same REE patterns as the leucotonalitic veins and mafic migmatites, respectively (Fig. 7a and d).

The metasedimentary migmatites display negative Eu anomalies ($Eu_N/Eu^*_N \sim 0{\cdot}71$), significantly high La_N/Yb_N ratios of around 75, and low concentration of the HREE ($Yb_N \sim 3$). The leucogranitic veins have patterns characterized by a distinct positive Eu anomaly and high La_N/Yb_N ratio (Fig. 7e); the main difference between the leucogranitic veins and their host metasedimentary migmatites is in the sign and value of the Eu anomaly.

Sr and Nd isotopic data

Samples for Sr and Nd isotopic analysis were selected to be representative of the rock types of each lithological unit and to encompass their range of major element compositions (Table 3 and Fig. 8). Overall, $\varepsilon_{Nd}(T)$ correlates negatively with $^{87}Sr/^{86}Sr(T)$ among rock types (Fig. 8).

Gabbroic rock (VFSJ10) has high $^{143}Nd/^{144}Nd(T)$ and low $^{87}Sr/^{86}Sr(T)$, consistent with its mineral and chemical composition. Furthermore, two out of three mafic migmatites are isotopically similar to the gabbroic rocks with $\varepsilon_{Nd}(T)$ values of +2·24 and −0·94 (calculated at 485 Ma, an average age for the Famatinian arc; e.g. Pankhurst *et al.*, 1998) and $^{87}Sr/^{86}Sr(T) < 0{\cdot}7063$. The other mafic migmatite (VFSJ11) has higher $^{87}Sr/^{86}Sr(T)$ and lower $\varepsilon_{Nd}(T)$ than the lithologically equivalent migmatites, similar to those of some leucotonalites, diorites and tonalites. It should, however, be noted that this mafic migmatite (VFSJ11) also has distinctively high LREE concentrations relative to the other mafic migmatites (Fig. 7a). The leucotonalitic veins have significantly higher $^{87}Sr/^{86}Sr(T)$ and lower $^{143}Nd/^{144}Nd(T)$ than their host mafic migmatites (compare specimens VFSA25A and 25B in Table 3).

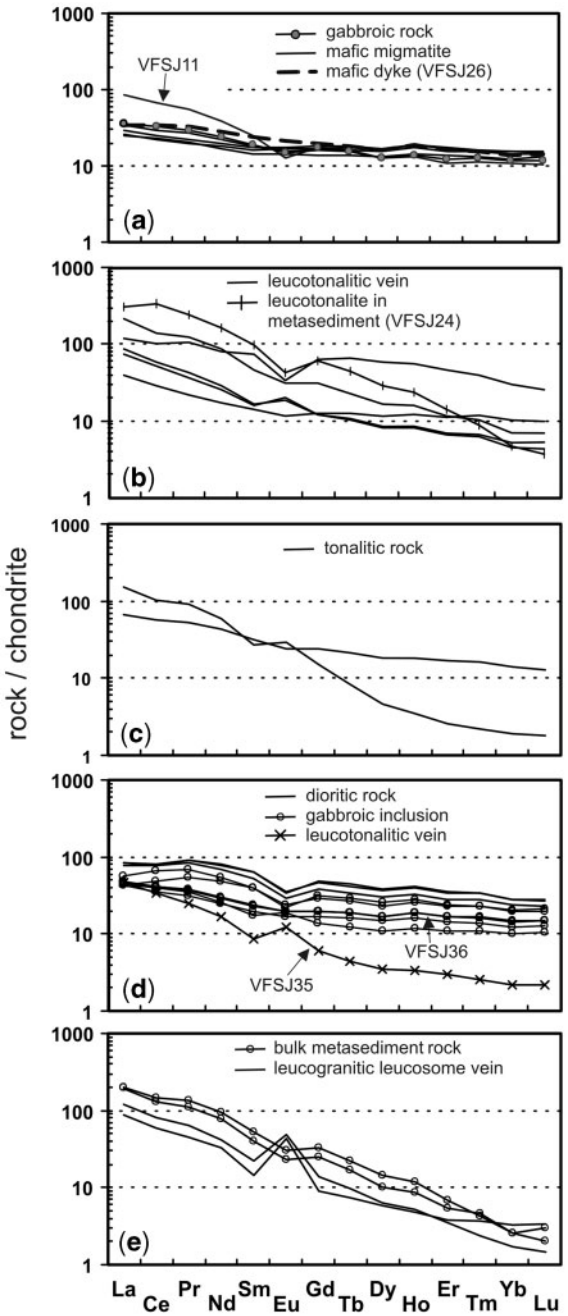

Fig. 7. Rare earth element abundances of igneous rocks and metasedimentary rocks normalized to C1 chondrite (Anders & Grevesse, 1989). (a) Gabbronorites from the mafic unit. (b) Leucotonalitic veins. (c) Tonalitic rocks from the transition between mafic and intermediate units. (d) Dioritic rocks, gabbroic blocks included in diorites, and a leucotonalitic vein separated from a mafic migmatite that is an inclusion in diorite (see text for further details and Fig. 3 for location). (e) REE whole-rock composition of the metasedimentary migmatites and leucogranitic leucosomes separated from them. REE data for representative metasedimentary migmatites are from Otamendi *et al.* (2009).

A leucotonalite (VFSJ15) has an isotopic composition close to those of the mafic migmatites. In contrast, two other leucotonalitic veins (VFSJ19 and 25A) have isotopic compositions more similar to those of the metasedimentary migmatite and anatectic leucogranite than to those of the mafic migmatites. Metasedimentary migmatites and the anatectic leucogranite are distinguished by a radiogenic isotopic composition that combines the highest $^{87}Sr/^{86}Sr(T)$ (>0·715) with the lowest $\varepsilon_{Nd}(T)$ (<−6·2).

The dioritic rocks from the intermediate unit have $\varepsilon_{Nd}(T)$ and $^{87}Sr/^{86}Sr(T)$ values of −4·36 to −5·54 and 0·709–0·712, respectively. Furthermore, the dioritic rocks form a cluster in the middle of the $\varepsilon_{Nd}(T)$–$^{87}Sr/^{86}Sr(T)$ array between the mafic and metasedimentary migmatites (Fig. 8). Compared with the dioritic rocks, the tonalitic rocks have slightly higher $^{87}Sr/^{86}Sr(T)$ and have similar $\varepsilon_{Nd}(T)$ values.

DISCUSSION

Partial melting of gabbroic rocks

Comparison with experimental results

The leucosome-forming process in the migmatites involves two interacting mechanisms: (1) melting reactions driven by the *P–T–t* trajectory; (2) segregation of melts assisted by the local strain rate (Sawyer, 1991). This is the central reason why it is difficult to separate leucosomes representing a pure melt composition and we are very unlikely to obtain leucosomes formed in equilibrium with their host mesosomes (Sawyer, 1991; Bea, 1996; among others). Furthermore, it is generally not possible to determine confidently the conditions of water activity and oxygen fugacity under which a migmatite formed. Within this context, experimental studies designed to determine phase equilibria yield the composition and fraction of melts (glasses) generated during progressive partial melting (e.g. increasing temperature and/or water activity). In general, these experimental results provide the best constraints against which natural rocks can be compared. The approach has been proved to be useful (e.g. Patiño Douce, 1999) even though the great majority of the igneous rocks, from narrow leucosomes to large plutons, crystallized from magmas (e.g. melt plus crystals) rather than from a pure melt.

To be strictly comparable, the natural rock parental to the migmatites should have the same composition as that of the starting material used in the experimental runs. Hence, the experimental data of Beard & Lofgren (1991) provide some useful constraints for this study because there is close compositional similarity between the hornblende hornfels 466 used as their starting material and the gabbroic rocks from our study area (Fig. 9). As illustrated in Fig. 9, the leucotonalitic veins have compositions broadly overlapping with the composition of glasses

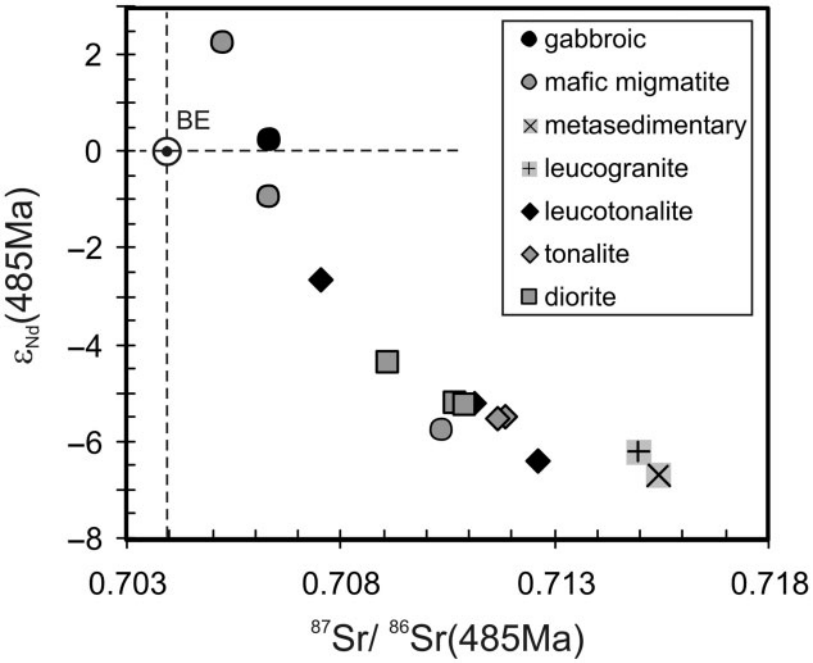

Fig. 8. Variation of ε_{Nd} vs $^{87}Sr/^{86}Sr$ at 485 Ma for rocks selected to be representative of the lithological diversity in the cross-section shown in Fig. 3.

produced by Beard & Lofgren (1991) by melting hornblende hornfels 466 at 3 and 6·9 kbar. This resemblance between the experimental materials and the natural rocks is taken to indicate that the leucotonalitic veins result primarily from partial melting of gabbroic rocks. In contrast, the medium-K hornblende gabbro (87S35A) investigated by Sisson *et al.* (2005) shows that melting a source with a medium-K high-alumina basaltic composition produces glasses with higher total alkali contents (Fig. 9a) and Peacock indices (Fig. 9b), but similar $MgO + FeO^*$ concentrations (see Fig. 9c) compared with our leucotonalitic veins. These differences can be explained as resulting from a total alkali content that is higher in the medium-K basalt (87S35A) than in the studied gabbroic rocks. These differences provide additional evidence for the idea that the leucotonalitic veins were derived from a source with a composition, at least in total alkali abundance, similar to that of the gabbroic rock.

Generation of the leucotonalitic veins by melting mafic rocks is also suggested by their close resemblance to the leucosomes of other mafic migmatites (e.g. Sawyer, 1991; Williams *et al.*, 1995). Compared with the other natural examples at similar SiO_2 contents, the studied leucotonalitic veins have slightly higher alumina saturation indices (Fig. 9d). However, the experimental glasses produced by melting mafic materials have even higher alumina saturation indices than the studied leucotonalites. Water fugacity in the partially melted rock has an indirect effect on the amount of Al_2O_3 in the resultant melts, because as Beard & Lofgren (1991) have shown, the relative contributions of amphibole and plagioclase to the melting reaction are determined by the fugacity of water. Compared with a water-saturated melting process, dehydration partial melting (i.e. all water supplied by hydrous minerals) is driven by an increased participation of hornblende relative to plagioclase, leading to melts depleted in Al_2O_3 (Beard & Lofgren, 1991; Fig. 14). From these results a simple conclusion can be reached: the leucotonalitic veins were generated by water-undersaturated melting; however, it cannot be asserted that the process of partial melting was driven only by hornblende dehydration.

Mass-balance constraints on melting reaction

Experimental results (Beard & Lofgren, 1991; Rushmer, 1991) predict that under water-undersaturated conditions mafic rocks partially melt following an incongruent melting reaction of the general form

$$\text{plagioclase} + \text{amphibole} \pm \text{quartz} \rightarrow \text{melt (tonalitic)} + \text{clinopyroxene} \pm \text{orthopyroxene}. \quad (1)$$

However, there is an inconsistency when the feasibility of this model reaction in supplying the amount of SiO_2 to form the leucotonalitic melt is tested from the point of view of mass balance. Quartz is absent or appears in small amounts in the gabbroic rocks representing the non-melted precursor, but a significant contribution of quartz

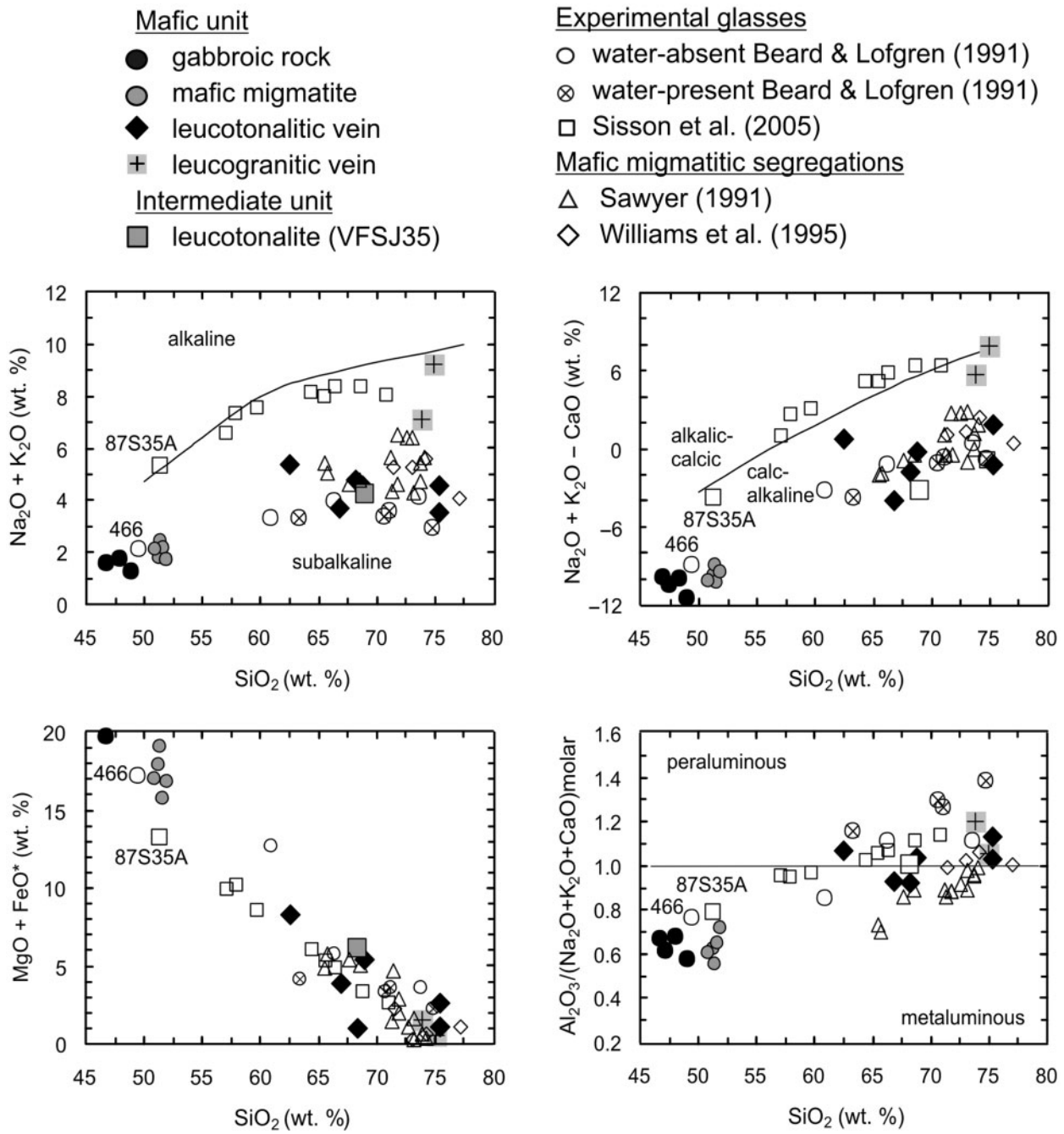

Fig. 9. Comparison of the major element composition of the leucotonalitic veins formed in the mafic migmatites with published data for both experimental melts and natural leucosomes formed by partially melting amphibole-bearing mafic rocks. Experimentally produced glasses are from Beard & Lofgren (1991) and Sisson *et al.* (2005); leucosomes from mafic migmatites are from Sawyer (1991) and Williams *et al.* (1995). The open circle numbered 466 and the open square numbered 87S35A show the starting composition used in the melting experiments of Beard & Lofgren (1991) and Sisson *et al.* (2005), respectively.

is required by this melting reaction (1). The required SiO_2 normally supplied by quartz can instead be released by the breakdown of plagioclase (e.g. Beard & Lofgren, 1991). However, this is not the case for the studied rocks because the gabbroic rocks contain plagioclase nearly always with greater than 80% anorthite with SiO_2 contents below 48 wt % (see also Otamendi *et al.*, 2009). Hence, there is a clear difficulty in generating leucotonalitic melts ($SiO_2 = 62–74$ wt %) if the reactants are only plagioclase ($SiO_2 < 48$ wt %) and hornblende ($SiO_2 \sim 45$ wt %).

Table 4: Stoichiometric coefficients for model melting reactions calculated through least-squares multiple regression

Model reaction (1): 0·4 Qtz + 0·33 Pl + 0·60 Amph → 1 melt (tonalitic) + 0·39 Cpx							
Mineral:	Qtz	Pl	Amph	Cpx	melt	Calc.	
Sample:		VFSJ10	VFSJ10	VFSJ15	VFSJ13	VFSJ13	r^2
SiO_2	100·0	44·80	46·93	51·55	62·47	62·47	0·00
TiO_2	0·00	0·00	0·68	0·16	0·86	0·35	0·26
Al_2O_3	0·00	35·11	10·79	2·01	17·14	17·32	0·03
FeO*	0·00	1·06	12·47	8·86	4·67	4·39	0·08
MgO	0·00	0·00	15·01	13·80	3·12	3·64	0·28
CaO	0·00	17·67	12·01	22·18	4·61	4·44	0·03
Na_2O	0·00	1·34	1·10	0·50	3·18	0·91	5·16
K_2O	0·00	0·02	0·84	0·00	2·20	0·51	2·84
Coefficient	0·40	0·33	0·60	−0·39	1·00	$\Sigma r^2 =$	8·68
Model reaction (2): 0·43 Qtz + 0·45 Pl + 0·26 Amph → 1 melt (tonalitic) + 0·16 Cpx							
Mineral:	Qtz	Pl	Amph	Cpx	melt	Calc.	
Sample:		VFSJ10	VFSJ10	VFSJ15	VFSJ15	VFSJ15	r^2
SiO_2	100·0	44·80	46·93	51·55	66·84	66·84	0·00
TiO_2	0·00	0·00	0·68	0·16	0·20	0·14	0·00
Al_2O_3	0·00	35·11	10·79	2·01	18·10	18·25	0·02
FeO*	0·00	1·06	12·47	8·86	2·48	2·16	0·10
MgO	0·00	0·00	15·01	13·80	1·10	1·52	0·18
CaO	0·00	17·67	12·01	22·18	7·52	7·43	0·01
Na_2O	0·00	1·34	1·10	0·50	3·27	0·80	6·10
K_2O	0·00	0·02	0·84	0·00	0·40	0·22	0·03
Coefficient	0·43	0·45	0·26	−0·16	1·00	$\Sigma r^2 =$	6·44
Model reaction (3): 0·63 melt (granitic) + 0·14 Pl + 0·34 Amph → 1 melt (tonalitic) + 0·13 Cpx							
Mineral:	leucogr	Pl	Amph	Cpx	melt	Calc.	
Sample:	VFSJ17	VFSJ10	VFSJ10	VFSJ15	VFSJ13	VFSJ13	r^2
SiO_2	73·82	44·80	46·93	51·55	62·47	62·43	0·00
TiO_2	0·11	0·00	0·68	0·16	0·86	0·28	0·33
Al_2O_3	13·93	35·11	10·79	2·01	17·14	17·25	0·01
FeO*	1·49	1·06	12·47	8·86	4·67	4·21	0·22
MgO	0·44	0·00	15·01	13·80	3·12	3·61	0·25
CaO	1·38	17·67	12·01	22·18	4·61	4·61	0·00
Na_2O	2·43	1·34	1·10	0·50	3·18	2·04	1·30
K_2O	4·69	0·02	0·84	0·00	2·20	3·26	1·12
Coefficient	0·63	0·14	0·34	−0·13	1·00	$\Sigma r^2 =$	3·24

*Total Fe given as FeO.

We address this quantitatively by attempting a major element mass balance for model melting reaction (1) using multiple least-squares regression (e.g. Le Maitre, 1979). Mineral compositions used for this calculation are given in Table 4, and the two leucotonalitic veins with lower SiO_2 contents are used as the melt composition. We are not implying that these veins are a better proxy for pure melts than the others, but if the mass balance of SiO_2 is

shown to be inadequate for them, it would be more difficult to model the other leucotonalites that have higher SiO_2 contents. As it is not possible that plagioclase + amphibole are the only reactants able to generate a leucotonalitic melt, quartz must be added as a reactant component [e.g. model reactions (1) and (2) in Table 4]. It should be noted that if quartz were not included, the mass-balance model would yield stoichiometric coefficients predicting that clinopyroxene is a reactant and amphibole is a product of the melting reaction.

The mass balance yields the expected position for both reactant and product minerals in the melting reaction (1), but the models using quartz + plagioclase + amphibole as reactants fail to reproduce the composition of typical leucotonalitic melts, because the computed sums of the squares of the residuals ($\Sigma R^2 > 6$) are too high to be statistically acceptable (see Table 4). Furthermore, the stoichiometric coefficients for these models imply that quartz must be consumed by reaction (1) according to a stoichiometric factor between that at which amphibole and plagioclase are also consumed. Given the scarce amount of quartz in the purported protoliths (gabbroic rocks), a quartz-consuming melting reaction would cease after generating a small fraction of melt. Besides the problem created by the deficiency of quartz, the compositions of the calculated leucotonalitic melts do not match those of the leucotonalitic veins. The larger divergence is related to the impossibility of replicating the abundance of Na_2O and K_2O in the leucotonalitic veins (see Table 4).

If the model partial melting reaction (1) is applied using the actual mineral compositions in the gabbroic rocks, the reactive phases are not able to supply the amount of alkalis and silica required to form the leucotonalitic veins. A leucogranitic melt involved as a reactant could, however, fill the deficiencies. The introduction of a leucogranitic melt significantly improves the mass balance, even though the concentrations of K_2O and Na_2O cannot be replicated with statistically acceptable accuracy [see model reaction (3) in Table 4]. The input of a leucogranitic melt into the mafic migmatites also resolves other contradictory observations. If, as field observations suggest, the gabbroic rocks are the protolith to the mafic migmatites, we cannot explain why they have generally lower silica and total alkali contents than the mafic migmatites. This contradicts the observation that partial melting and melt segregation deplete the silica and alkali content of the residue relative to the non-melted protolith. Because at a regional scale the gabbroic rocks have no or little quartz (e.g. Otamendi *et al.*, 2009), the assumption that the pre-melted mafic protolith had more quartz than the non-melted gabbroic rocks is less tenable than the idea of an input of leucogranitic anatectic melt catalyzing the partial melting of the gabbroic rocks. We, thereby, propose that the melting process that generated the leucotonalitic veins and the mafic migmatites is better represented by an open-system partial melting process:

$$\begin{aligned}&(\text{plagioclase} + \text{amphibole})\ \text{gabbroic rock} + \\ &\quad \text{leucogranitic melt} \rightarrow \text{leucotonalitic melt} + \\ &\quad \text{clinopyroxene} \pm \text{orthopyroxene}\end{aligned} \qquad (2)$$

in which the leucogranitic veins sourced from the metasedimentary migmatites and intruded into the gabbroic packages are the leucogranitic melt involved as a reactant in the model reaction (2).

The origin of leucotonalitic veins in the mafic migmatites

Rare earth element abundances and modelling

The leucotonalitic veins have distinctive REE patterns that vary between two end-members, which show significant differences in their total REE contents (Fig. 7). Leucogranitic veins with high La_N/Yb_N ratios and positive Eu anomalies represent the low ΣREE end-members, whereas the leucotonalitic vein with high ΣREE, low La_N/Yb_N and a negative Eu anomaly lies at the other compositional extreme. These differences suggest that at least two processes have governed the REE characteristics of the leucotonalitic veins. This is a common observation in leucosome magmas found within, or close to, their source (e.g. Sawyer, 1987; Barnes *et al.*, 2002). Hence, each study of a natural example has the problem of discerning which leucosome composition better approximates the most pure melt formed by partial melting. As shown above using major elements, all the leucotonalitic veins have compositions resembling experimental glasses, therefore major element variations cannot provide evidence for resolving this question. Although the results of REE modelling are useful in constraining the origin of the leucotonalitic veins some uncertainties remain until we discuss the results of isotopic modelling.

The behaviour of trace elements during partial melting can be modelled considering (1) equilibrium, (2) fractional or (3) disequilibrium melting, using conventional equations and making a number of assumptions (see Allègre & Minster, 1978; Sawyer, 1991). The REE concentration of the leucotonalitic veins with low ΣREE and a positive Eu anomaly cannot be modelled by any of the melting equations. However, if a disequilibrium melting process were originally responsible for the formation of the low ΣREE leucotonalitic leucosomes, and at the same time these leucotonalitic melts mixed with leucogranitic magmas sourced from the metasedimentary rocks, the final model liquid would broadly replicate the composition of the leucotonalitic veins with low ΣREE.

The equation for estimating the trace element distribution between melts and residual solids resulting from disequilibrium melting is taken from Sawyer (1991).

The concentration of REE i in the liquid (C_L^i) is given by $C_L^i = C_O^i\ (M^i/Q^i)$, with $M^i = (x_1 + Kd_2x_2 + \ldots\ Kd_nx_n)/Kd_1$, and $Q^i = (X_1 + Kd_2X_2 + \ldots\ Kd_nX_n)/Kd_1$. The initial concentration of REE in the source rock (C_O^i) is obtained from the gabbroic rock (VJSJ10). The partition coefficients (Kd_n) of REE between minerals and the melt are from Dunn & Sen (1994) for plagioclase, Klein *et al.* (1997) for amphibole, and Rollinson (1993) for clinopyroxene. The weight fraction of minerals in the source (X_n) is estimated from the modal proportions in the gabbroic rock. The weight proportions of minerals in the source are: 51% of amphibole, 35% of plagioclase, 10% of orthoyproxene, 3% of clinopyroxene, <1% of quartz. The weight fractions of minerals entering the melt (x_n) are estimated from mass-balance calculations [Table 4, model melting reaction (3)] that yield a rate of consumption of 0·14 for plagioclase and 0·34 for amphibole as reactants to form melt plus clinopyroxene at a rate of 0·13. It should be noted that because the mass-balance estimates are used to constrain the stoichiometry of the melting reaction, the source rock includes orthopyroxene that is neither reactant nor product, and hence is regarded as an 'inert' phase. Initially, the melting reaction produces only 37% of the melt forming the veins, but the result obtained considering disequilibrium melting is significant in that the composition of the model liquid closely matches the concentration of some MREE and HREE in the low ΣREE leucotonalitic veins (Fig. 10a). Furthermore, the REE pattern predicted by disequilibrium melting has a shape similar to that of the leucotonalitic vein with the lowest total REE abundance (VFSJ15). A better fit to the low ΣREE leucotonalite vein is obtained when the melt generated by disequilibrium melting is mixed with a leucogranitic vein in a ratio 0·37:0·63 as predicted by mass balance (e.g. Table 4). As Figure 10b illustrates, the final model liquid has lower MREE and HREE concentrations than the low ΣREE leucotonalitic veins, but the slope and shape of the REE pattern is similar. Furthermore, the model replicates the positive Eu anomaly of these leucotonalitic veins, even though the anomaly is more pronounced in the model than in the veins (Fig. 10b).

The leucotonalitic veins with high ΣREE contents have negative Eu anomalies, whereas those with low ΣREE have positive Eu anomalies, suggesting that plagioclase fractionation controlled the REE behaviour (Fig. 7). The leucotonalitic vein with the lowest ΣREE has no Eu anomaly and a smooth REE pattern. Thus, this leucotonalite (VFSJ15) may be regarded as the closest approximation to the original melt composition (e.g. Sawyer, 1991). This assumption is consistent with the isotopic signature of the leucotonalites, which is discussed below. Therefore, we proceed to model the origin of the leucotonalitic veins with high total REE by assuming that the leucotonalitic vein with the lowest ΣREE was the primary melt from which

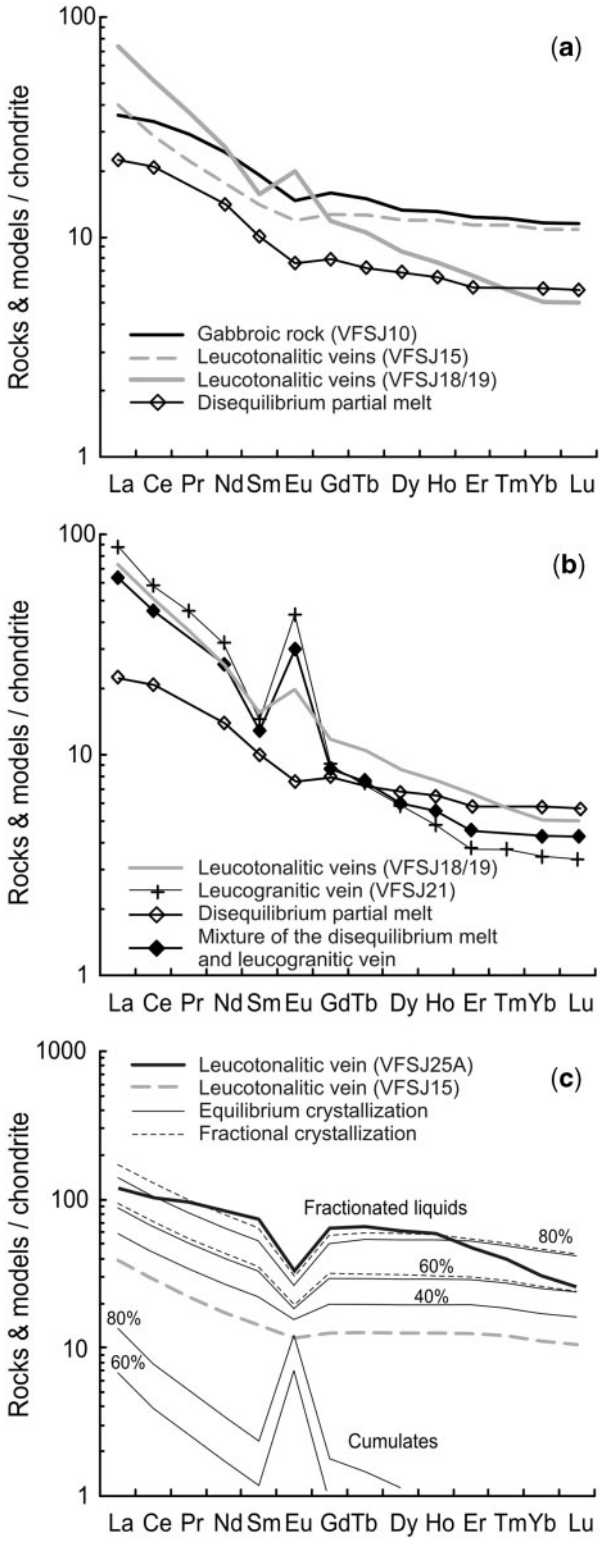

Fig. 10. Chondrite-normalized REE diagrams showing the results of the numerical simulation of partial melting and fractional crystallization. (a) Disequilibrium partial melting of gabbroic rock (VFSJ10). (b) REE model composition that results from mixing 63% of the anatectic leucogranite VFSJ21 and 37% of the disequilibrium partial melt. (c) Equilibrium crystallization of leucotonalic vein VFSJ15 (dashed grey line), showing the range of fractionated melts and cumulate compositions estimated by varying the degree of crystallization from 40 to 80% and considering both equilibrium and fractional crystallization models.

the other leucotonalitic veins were derived. Figure 10c shows the REE contents of both fractionated liquids and cumulates formed by the crystallization of plagioclase. Crystallization models indicate that the observed range of REE contents of the leucotonalitic veins with high ΣREE (VFSJ25A) can be derived by crystal fractionation starting from a parent melt with total REE abundance similar to the vein with the lowest ΣREE (VFSJ15). A puzzling aspect is that, even though the leucotonalitic veins with high ΣREE can be fractionated magmas, the complementary cumulates have not been positively identified.

Mixing of isotopically distinct sources during partial melting

The Nd–Sr isotopic compositions of the leucotonalitic veins are highly variable, and overlap with the composition of one of the mafic migmatites (Fig. 8). These isotopic compositional relationships are taken to indicate that the leucotonalitic veins and the mafic migmatites cannot be melt–residuum complementary pairs formed by closed-system equilibrium partial melting. Isotopic disequilibrium has been found to occur frequently during partial melting of metapelitic assemblages (Barbero *et al.*, 1995; Zeng *et al.*, 2005). Because isotopic equilibration is reached faster than elemental equilibration, disequilibrium of the radiogenic isotopic systems would also be associated with trace element disequilibrium during partial melting and melt segregation (e.g. Barbero *et al.*, 1995). In this study, mass-balance calculations and REE modelling suggest that partial melting was both a disequilibrium and an open-system process [e.g. reaction (2)].

As shown in Fig. 11a and b, only one (VFSJ15) of the three leucotonalitic veins for which isotopic data are available shows similar $^{87}Sr/^{86}Sr(T)$ and $^{143}Nd/^{144}Nd(T)$ to the gabbroic rock and the mafic migmatites, whereas the other two leucotonalitic veins are isotopically distinct. These may reflect the contribution of sources with different isotopic compositions to the formation of the leucotonalitic veins within the mafic migmatites. In Fig. 11a and b, $^{87}Sr/^{86}Sr(T)$ and $^{143}Nd/^{144}Nd(T)$ are plotted against the abundances of the parent elements Sr and Nd, respectively; calculated mixing curves between gabbro and leucogranite and metasediment are indicated (see Langmuir *et al.*, 1978). Two analyzed leucotonalitic veins (VFSJ19 and 25A) and one mafic migmatite (VFSJ11) have isotopic compositions falling close to the mixing lines. The mixing calculation indicates that these rocks (VFSJ19, 25A and 11) contain more than 50% of the leucogranite or metasediment end-member, consistent with elemental mass-balance calculations (see Table 4). Further tests for the isotopic sources contributing to form the leucotonalitic veins may be developed based on isochron diagrams (e.g. Faure, 1986). Two fictitious isochrons are drawn in Fig. 11c between the gabbroic rock and either the leucogranitic vein or the metasedimentary rock. The leucotonalitic veins do not lie along either of these fictitious isochrons. However, they display an isotopic trend similar to that of the fictitious isochrons. Thus, the isochron diagram can be resolved into a broad diagonal array of data. The array is interpreted as a mixing trajectory because the data cannot be fitted to any isochron constructed using an age of 485 Ma, which is the average age for the Famatinian magmatism (Fig. 11c). Furthermore, the isotopic compositions of the leucotonalitic veins and of one mafic migmatite (VFSJ11) cannot be related by radiogenic isotopic decay to the gabbroic rock. In contrast, the metasedimentary rock and the leucogranitic veins plot on an isochron constructed at 485 Ma, clearly supporting a genetic link between these two rocks.

Generation of tonalitic and dioritic rocks

Tonalitic and dioritic rocks are not fractionation products of less-evolved mafic (gabbroic) magmas. The most obvious evidence against a closed-system process is that the tonalitic and dioritic rocks have higher $^{87}Sr/^{86}Sr(T)$ and lower $^{143}Nd/^{144}Nd(T)$ than the gabbroic rocks and mafic migmatites from the same sequence (Fig. 8). It is here important to recall that in the field we can track the tonalitic system from a diffuse narrow leucosome to a discrete body (Figs 3–5), which suggests that there is a genetic link between the leucotonalitic veins and the tonalitic and dioritic intrusive bodies. Isotopic data are consistent with this hypothesis because the Sr- and Nd-isotopic compositions of the tonalitic and dioritic rocks are within the range of those of the leucotonalitic veins (Fig. 8). However, the implicit idea that the leucotonalitic veins are the parental magmas to tonalitic or dioritic magma bodies has to explain compositional variations that would be unexpected in terms of those predicted by a typical igneous evolutionary trend. Considering the range of possible indices of differentiation (e.g. Cox *et al.*, 1979), the leucotonalitic veins have more-evolved major element compositions than the tonalitic and dioritic rocks forming the intrusive bodies (Fig. 6a–d).

The hypothesis that the leucotonalitic veins are parental melts to the tonalitic and dioritic magma bodies needs to explain how the leucotonalitic veins have regressed to produce the tonalitic and dioritic rocks. The petrological problem is illustrated when the compositions of the rocks are plotted on two-element variation diagrams together with representative mineral compositions. Figure 12a clearly shows that any combination of fractionating mineral phases not involving quartz as the dominant phase cannot drive a fractionation trend that moves the melt composition from leucotonalite through tonalite to diorite. Furthermore, the possibility that quartz could be a major fractionating mineral would be regarded as a rare case in which early quartz crystallization chemically leverages the effect produced by crystallizing distinct combinations of amphibole, pyroxenes, and plagioclase (Fig. 12a). As an

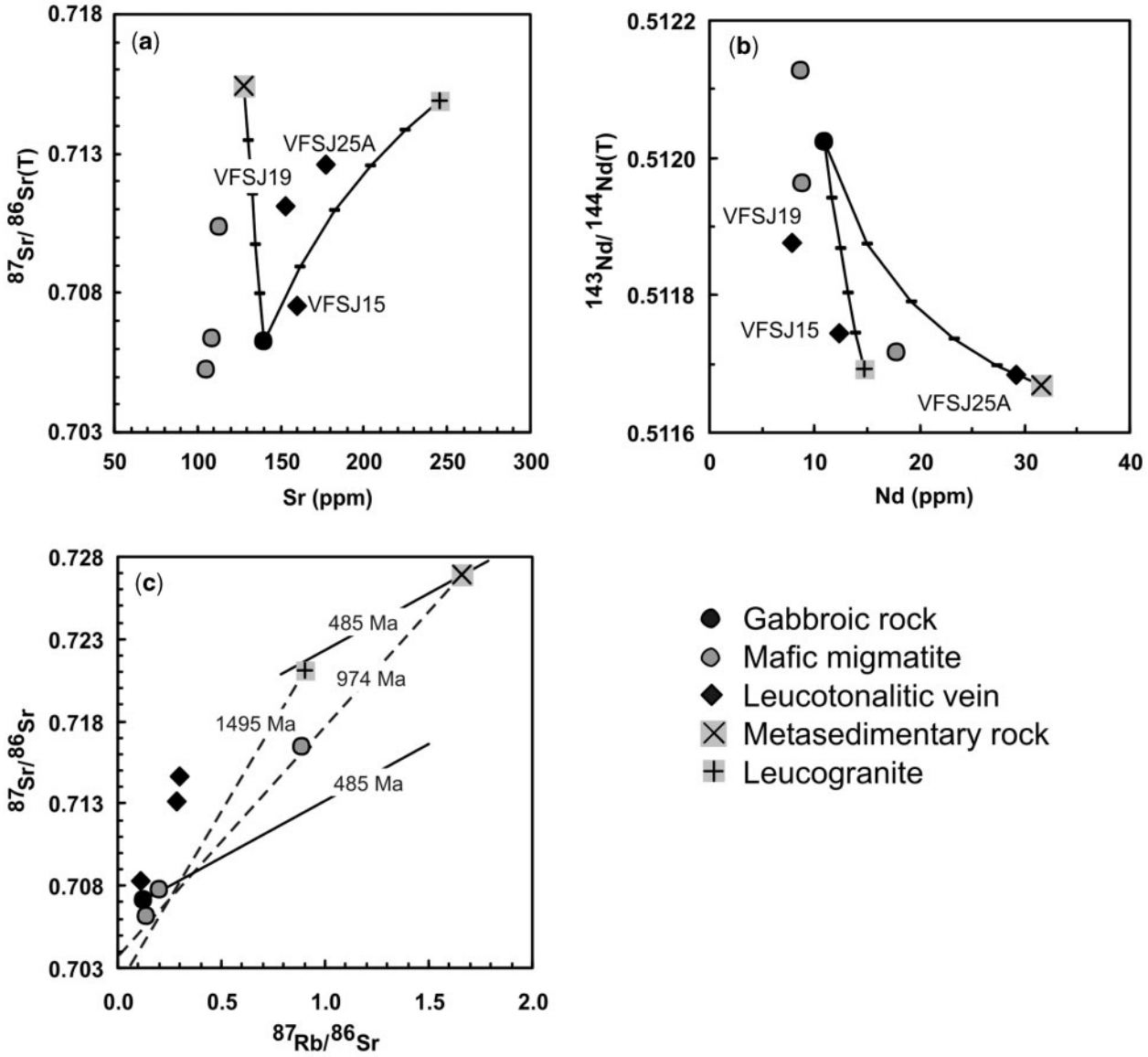

Fig. 11. (a) $^{87}Sr/^{86}Sr$ vs Sr for gabbroic rock, mafic migmatites, leucotonalitic veins, metasedimentary migmatites and anatectic leucogranites. (b) the same rocks as in (a) on a $^{143}Nd/^{144}Nd$ vs Nd diagram. Mixing lines for mixtures of the gabbroic rock and either the metasedimentary rock or the leucogranite are indicated in (a) and (b). (c) Two fictitious Rb–Sr isochrons indicated by dashed lines computed using the same end-members as in (a) and (b). The numbers shown on each isochron are the calculated fictitious ages. An isochron calculated at 485 Ma is shown for comparison.

alternative, one petrogenetic process that could give rise to regression of the magma composition is assimilation of less-evolved materials; in this example, the leucotonalitic veins that coalesce into magma bodies would have had to assimilate their entrained blocks of gabbroic and mafic migmatitic rocks. This does, however, create a thermal problem, which will be discussed further below.

Tonalitic and dioritic rocks have compatible trace element contents more similar to the gabbroic rocks and mafic migmatites, but incompatible lithophile element abundances (Ba, Rb, and K) closer to the metasedimentary migmatite compositions than their supposed parental leucotonalitic veins. On diagrams illustrating the variation of either compatible trace elements (Sc) against MgO (Fig. 12b) or incompatible elements (e.g. Ba and Rb) against K_2O (Fig. 12c) the tonalitic and dioritic rocks plot in the middle of a single linear trend. The mafic migmatites and gabbroic rocks always form one end-member to this trend, but the other end-member changes. Whereas the leucotonalitic veins are the end-member when compatible elements are plotted (Fig. 12b), metasedimentary migmatites define the extreme of the trend when

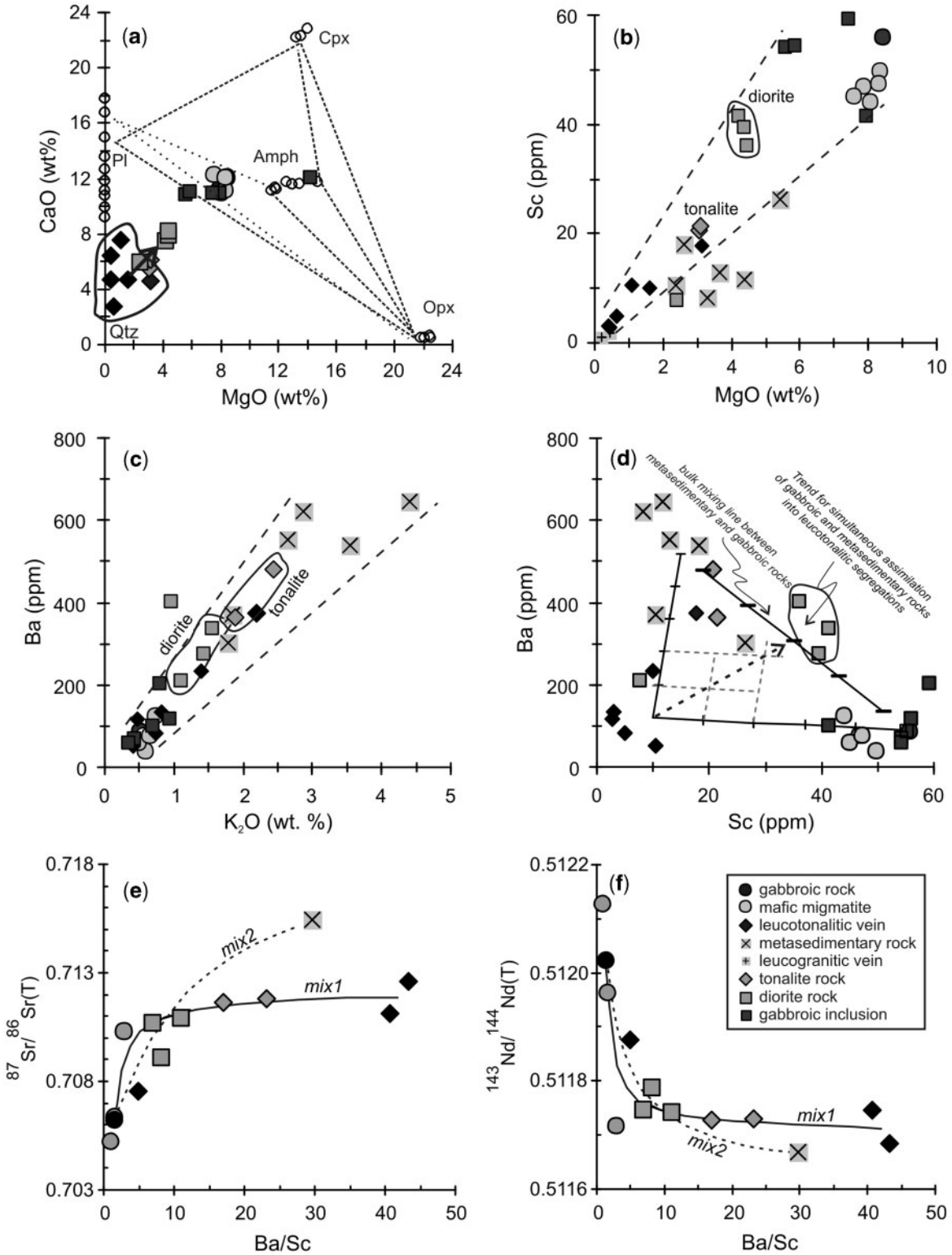

Fig. 12. (a) MgO vs CaO variation diagram showing that neither the pre-melting assemblage Pl ($\sim An_{80}$) + Amph + Opx joined by a dotted line, nor the residual assemblage Pl ($\sim An_{60}$) + Amph + Opx + Cpx outlined by a dashed line can explain the chemical trends of increasing MgO and CaO from leucotonalitic veins to tonalitic and dioritic rocks. (b) Sc vs MgO variation diagram for tonalitic and dioritic rocks and their surrounding lithologies. (c) Ba vs K_2O variation diagram for tonalitic and dioritic rocks and their surrounding lithologies. In (b) and (c) the dashed lines are arbitrarily drawn to show that the tonalitic and dioritic rocks fall on a mixing array with distinct end-members. (d) Ba vs Sc variation for tonalitic and dioritic rocks and their surrounding lithologies. Continuous lines show bulk mixing between distinct end-members. Tick marks on the lines represent 20% mixing intervals. The dashed arrow shows the evolutionary trend followed by a typical leucotonalitic melt that assimilates equal amounts of gabbroic and metasedimentary rocks. (e) Plot of $^{87}Sr/^{86}Sr$ at 485 Ma vs Ba/Sc for tonalitic and dioritic rocks and other lithologies that may be parental to them. (f) Plot of $^{143}Nd/^{144}Nd$ at 485 Ma vs Ba/Sc. In the ratio–ratio plots (e) and (f) the mixing hyperbolae are computed following the procedure of Langmuir *et al.* (1978). Mixing models test two hypotheses: model *mix1* for mixtures of the gabbroic rock and leucotonalitic veins; model *mix2* for mixtures of the gabbroic rock and a typical metasedimentary migmatite.

incompatible elements are used (Fig. 12c). These elemental variations suggest that at least three sources are involved in generating the chemical composition of the intermediate rocks.

Figure 12d illustrates in terms of trace elements that the composition of the tonalitic and dioritic rocks might be the result of two distinct processes, bulk mixing between gabbroic rocks or mafic migmatites and metasedimentary migmatites, or simultaneous assimilation of mafic and metasedimentary migmatites into the leucotonalitic magmas. Ratio–ratio variation diagrams, in which Sr and Nd isotopic composition is plotted against Ba/Sc (e.g. Langmuir *et al.*, 1978), help to better constrain the composition of the precursor involved in the generation of the tonalitic and dioritic rocks. Figure 12e and f shows a test for comparing between the two alternative mixing processes. In these two-component mixing models, one end-member is always the gabbroic rock, whereas the other end-member is either the leucotonalitic veins with highly radiogenic Sr compositions (curve *mix1*) or the metasedimentary migmatite (curve *mix2*). The most significant difference between the mixing models is that the composition of the tonalitic rocks cannot be accurately replicated when the composition of the metasedimentary migmatite is used as a mixing end-member. However, either mixing model can reproduce the composition of the diorites. The relevant result is that the elemental and isotopic composition of the tonalitic and dioritic rocks can be explained by hybridization of rocks that are spatially associated with them. Most of the fragments assimilated by the leucotonalitic magmas may have remained in the solid state during physical mingling and chemical mixing (e.g. Beard *et al.*, 2005). Incompletely assimilated blocks of mafic and metasedimentary rocks in the dioritic and tonalitic rocks support this idea (Fig. 5e and f). Therefore, commingling between the leucotonalitic magmas and solid rock fragments entrained in them, and subsequent true mixing, is believed to have occurred after the leucotonalitic veins coalesced to form small, but discrete, magma bodies.

The possibility that the tonalitic and dioritic rocks were generated at deeper crustal levels by the fractional crystallization of gabbroic magmas and concurrent assimilation of metasedimentary migmatites (i.e. AFC) cannot be ruled out on isotopic grounds. Choosing appropriate values for the bulk partition coefficients and rates of assimilation to fractional crystallization, the equation for modelling the AFC process would yield theoretical trends similar to those of mixing (*mix2*). This conclusion is valid regardless of the petrogenetic model, which may be either mass- or energy-constrained (e.g. DePaolo, 1981; Bohrson & Spera, 2001). If we follow this approach, then the interpretation of the isotopic and trace element data cannot be constrained by field observations.

The thermal problem associated with the assimilation of mafic inclusions into the leucotonalitic magmas will now be addressed with qualitative arguments. The question is: how much, if any, relative mass of solid mafic fragments can be assimilated by the silicic leucotonalitic magmas? This issue has been addressed previously using experimental data and theoretical models (e.g. Beard *et al.*, 2005; García-Moreno *et al.*, 2006). These studies showed that water-bearing silicic melts are effective agents for assimilating solid fragments entrained in them. Significantly, the studies stress the fact that the agent of assimilation has a solidus temperature lower than that of the mineral assemblage in the solid assimilant (see Beard *et al.*, 2005; García-Moreno *et al.*, 2006). The capacity to assimilate is determined by the physico-chemical state (P–T–X_{H2O}) of the melt. At a given H_2O content in the melt, the potential for assimilation increases with either increasing T or decreasing P (e.g. García-Moreno *et al.*, 2006), as the melt moves further from its solidus (Holtz *et al.*, 2001). The process of assimilation depends upon the ambient temperature at which the process takes place; this dependence is commonly proportional to crustal depth. We envisage that the leucotonalitic magmas and their entrained solid inclusions were at the same temperature. In turn, the temperature was externally controlled, so that the process of assimilation was nearly adiabatic.

The ambient temperature in the deep crust of magmatic arcs is mainly controlled by the rate of under- and intraplating of mafic magma (Annen & Sparks, 2002; Jackson *et al.*, 2003; Dufek & Bergantz, 2005; Annen *et al.*, 2006). Although deep crustal levels are heated by under- and intra-plating mafic magma, a thick section of the lower crust will evolve under ambient temperatures higher than 750°C. The ambient temperature of the crustal levels in which the metasedimentary and mafic migmatites underwent partial melting to form leucotonalitic magmas has been estimated to be around 805 ± 35°C (Otamendi *et al.*, 2008, and unpublished data). Within this temperature range and at pressures from 2 to 8 kbar, the plagioclase + quartz + melt assemblage has a wide stability field in the $Ca_2Al_2Si_2O_8$–$NaAlSi_3O_8$–$KAlSi_3O_8$–SiO_2–H_2O system (e.g. Whitney, 1975). It follows that as long as the temperature remains constant, the melt fraction in a bulk leucotonalitic composition is mainly dependent upon the fraction of dissolved water in the melt (Holtz *et al.*, 2001). As a haplotonalitic bulk composition may consist of a large melt fraction under the P–T conditions of interest, two observations are crucial to understanding that silicic leucotonalitic magmas may assimilate relatively large masses of solid mafic fragments. First, the mechanism of assimilation would be one of hydration crystallization (e.g. Beard *et al.*, 2004). In such a case, the solid inclusions would not be melted; rather, they are physically disintegrated and then chemically mixed with the magma (Beard *et al.*,

2005). Second, the heat loss experienced by the leucotonalitic magmas during assimilation of solid fragments with a higher solidus temperature would be buffered by the ambient temperature, which, in a hot crustal zone, is imposed by the rate of intrusion of juvenile magma (Annen & Sparks, 2002; Dufek & Bergantz, 2005; Annen *et al.*, 2006). We found these conditions to be favourable for large amounts of mafic solid fragments to be assimilated into the leucotonalitc magmas. During the process of assimilation the host melt becomes enriched in CaO, FeO, and MgO, and depleted in SiO_2 (e.g. García-Moreno *et al.*, 2006); consequently, the dissolution of gabbroic inclusions into the leucotonalitic magmas would increase the solidus temperature of the magmatic system. Thus, we argue that the leucotonalitic magmas were in fact able to assimilate fragments of gabbroic rocks and mafic migmatites until their compositional regression led them to reach the solidus of the magmatic system.

Working model for generation of intermediate magmas in the deep arc crust

Based on the previous discussion, a major interpretation of our study is that tonalitic and dioritic rocks are the end-products of multi-stage petrogenetic processes involving several sources (Fig. 13). Three major stages are recognized in the formation of intermediate magmas: (1) sustained influx of hydrous mafic magmas into a region of the deep crust that contains metasedimentary rocks; (2) physically and chemically coupled melting of mafic and metasedimentary rocks and formation of the leucotonalitic veins and dykes, which coalesce to form larger magma bodies; (3) homogenization and blending (hybridization) of several lithologies in discrete magma bodies where the leucotonalitic magmas undergo compositional regression after assimilating their mafic and metasedimentary precursors. These stages should follow sequentially because the magmas and their associated crystalline rocks are processed in sequence, even though at the scale of the arc crust more than one stage of the process may be operating at the same time. As illustrated in Figs 13 and 14 the main changes associated with each stage resulting in intermediate magmas would involve the following processes.

(1) Long-lasting ($>10^5$ Myr; e.g. Jackson *et al.*, 2003; Dufek & Bergantz, 2005; Annen *et al.*, 2006) intrusion of mantle-derived mafic magmas into a region of the deep crust containing fertile metasedimentary rocks provides both the thermal energy and the material required for the generation of intermediate magmas. An important observation for this initial stage is that the continuous flux of hydrous mafic magma leads to thick supra-solidus packages of fertile metasedimentary rocks (Bergantz, 1989; Jackson *et al.*, 2003). According to this model, the metasedimentary packages residing in deep crustal levels of the arc undergo partial melting under fluid-undersaturated conditions. Although our study provides only an outcrop-scale view of the partial melting of the metasedimentary migmatites, the existence of crustal-scale anatectic leucogranitic magmas has been documented by the mapped extension of anatectic leucogranites into their parental metasedimentary migmatites (e.g. Otamendi *et al.*, 2008). Leucogranitic melts sourced from the metasedimentary migmatites then intrude into the surrounding gabbroic rocks (Fig. 5c).

(2) Partial melting of amphibole-rich gabbroic rocks may occur independently of partial melting in the adjoining metasedimentary packages (e.g. Sawyer, 1991; Williams *et al.*, 1995). It is not possible to determine in the field whether before beginning to melt the gabbroic rocks were either already below their solidus or at supra-solidus but close to solidus temperatures. However, the study area abounds with examples from outcrop to regional scale that document the partial melting of the mafic rocks to be physically coupled with the formation of metasedimentary migmatites. This observation may indicate that, when compared with partial melting of pure mafic (gabbroic) protoliths, coupled partial melting would produce more melt because the fusible components (silica, alkalis and fluids) are transferred through the gabbroic rocks by melts released from the adjacent metasedimentary rocks (e.g. Skjerlie & Patiño Douce, 1995). A significant amount of melt (*c.* 30% of the mass of gabbroic plus metasedimentary rocks) would be generated if ambient temperatures were around $820^\circ C \pm 20^\circ C$ (Skjerlie & Patiño Douce, 1995). The net result of the coupled melting processes is to generate magmas with a dominant leucotonalitic composition, sourced from the mafic rocks, rather than with a leucogranitic composition, sourced from the metasedimentary rocks.

(3) At the thermal conditions of melt generation and after being drained from the source, the leucotonalitic veins would contain melt-dominated magmas that coalesce to form bodies tens of metres thick. The leucotonalitic magmas evolve at temperatures well above their water-saturated solidus, so they would be able to react, commingle, and mix with the solid inclusions entrained in them (e.g. Beard *et al.*, 2005). These magma bodies would have melt-dominated rheological behaviour (Vigneresse *et al.*, 1996). Stirring of the entrained solid inclusions in these magma bodies led to fragmentation of the solid inclusions. Then, these fragmented mafic or metasedimentary inclusions were assimilated to variable degrees by reaction with the host leucotonalitic magma (see Beard *et al.*, 2004). In mineralogical and chemical terms, this process leads to a compositional 'regression' as the leucotonalitic magmas become tonalitic and then dioritic in composition; the difference between the tonalites and diorites is thus one

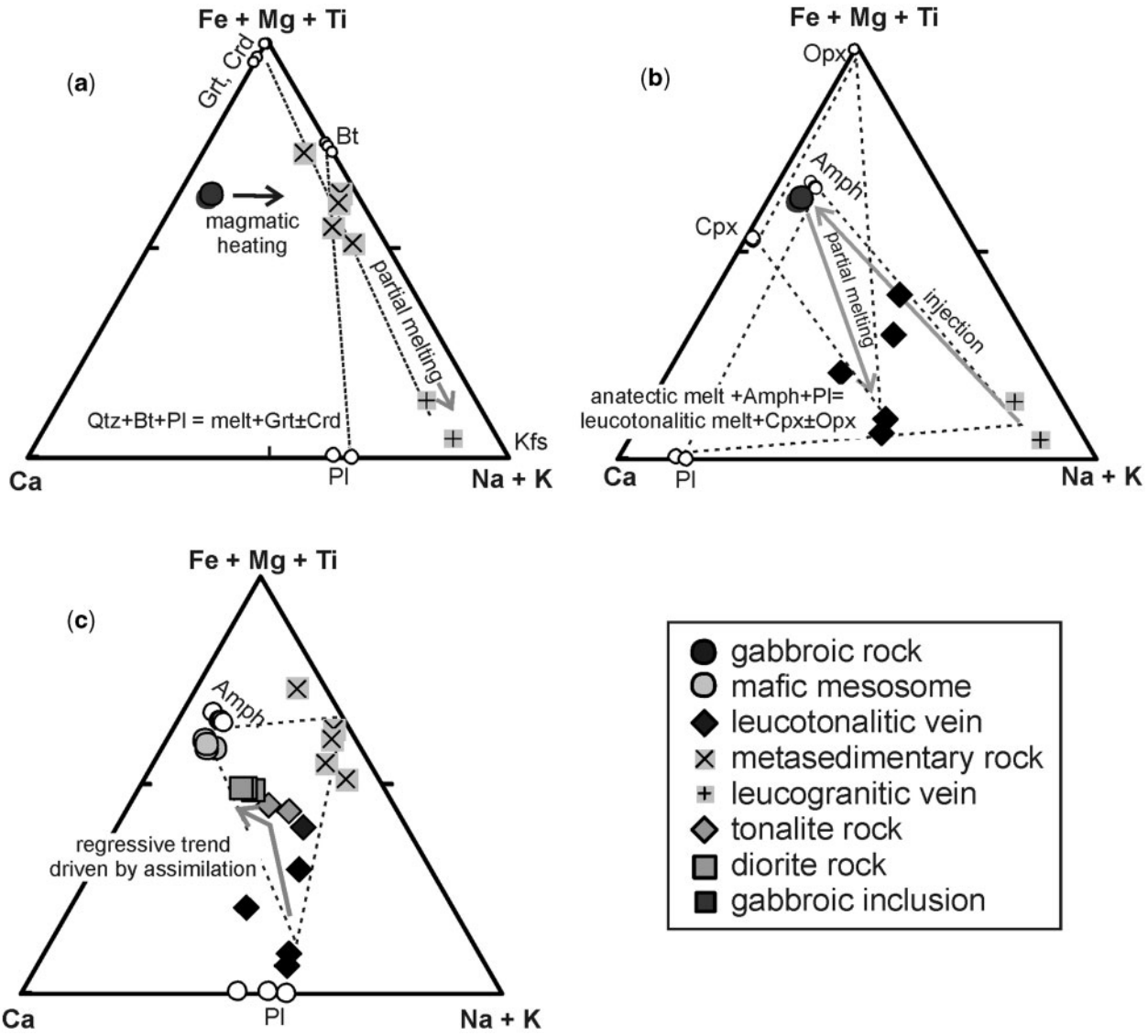

Fig. 13. The main stages of the petrogenetic evolution of the leucotonalites shown as compositional variations in terms of (Fe + Mg + Ti), (K + Na), and Ca, cation proportions. (a) Intrusion of mafic magma into supracrustal metasedimentary rocks and its crystallization to form gabbroic rocks promotes water-undersaturated melting of the metasedimentary packages. Dashed tie-lines connect the reactants (Bt + Pl) and products (Kfs + Grt ± Crd) of the melting reaction, with mineral composition after Otamendi *et al.* (2008) and unpublished data. (b) Injection of leucogranitic dykes into the gabbroic rock enhances partial melting in the gabbroic layers. Leucotonalitic veins form as the net result of coupled melting of gabbroic and metasedimentary rocks. The tie-lines outline the reactants and the products of the melting reaction Amph + Pl + leucogranitic melt → Opx + Cpx + leucotonalitic melts. (c) When the coalescence of leucotonalitic veins formed small magma bodies, the leucotonalitic melts began to react and assimilate solid block of gabbroic rocks, mafic migmatites and metasedimentary migmatites. The dashed tie-lines join the three components involved in the generation of tonalitic and dioritic magmas.

of the amount of the mafic precursor assimilated by the leucotonalitic magma.

A final problem is that the dimensions of the source zone studied in the field seem to be insufficient to generate crustal-scale volumes of intermediate plutonic rocks (Fig. 14). In recognition of this, we accept the idea that other magma generation processes must also contribute to the formation of large-scale intermediate plutons in magmatic arcs. In particular, the Famatinian paleo-arc crust exposes only those magma source zones that were 'frozen in' by the tectonic closure of the arc while they were still active. We argue that a time-integrated perspective would show that early active source zones were subsequently cannibalized during the downward expansion of the plutonic bodies dominated by intermediate igneous rocks (see Fig. 14).

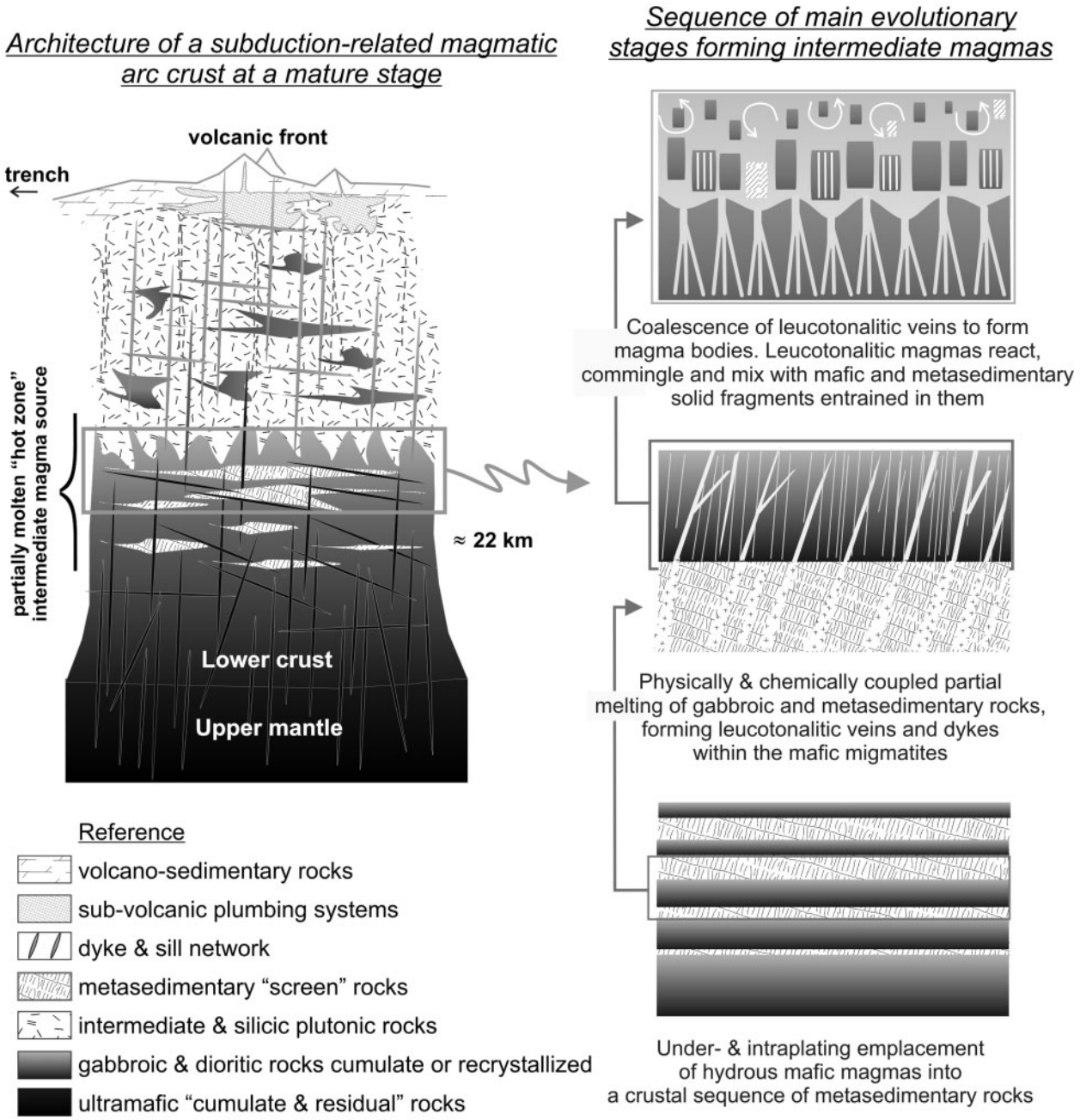

Fig. 14. Schematic stratigraphic column underlying the volcanic front of a mature magmatic arc (not to scale). The stratigraphy is reconstructed on the basis of exposed sections from the Famatinian paleo-arc and using sources cited in the text. At levels deeper than around 22 km the column is simplified after Dufek & Bergantz (2005) and Hollister & Andronicos (2006). The stratigraphic column incorporates a partially molten 'hot zone' as proposed by Annen *et al.* (2006). Within this partially molten zone occur the main petrogenetic processes contributing to the dioritic and tonalitic magmas as schematically depicted on the right side of the column.

Comparison with other Cordilleran systems

The Ordovician Famatinian arc in the central Andes is a Cordilleran-style arc, similar to the Mesozoic to modern arcs straddling the western margins of South and North America. It was developed on a continental upper plate during oceanic subduction along the margin of Gondwana (Pankhurst *et al.*, 1998) and it is characterized by the presence of a wide range of calc-alkaline plutonic bodies and volcanic rocks that have an average tonalite to granodiorite composition similar to Cordilleran arcs (e.g. Silver & Chappell, 1988). The Famatinian arc segment

exposed in the Sierra Valle Fértil–La Huerta is structurally most similar to the Cordilleran interior batholiths (Barton, 1996) that form sequences of paleo-horizontal magmatic sills emplaced into continental metasedimentary wall-rocks. These arcs (e.g. the Sierra Madre Occidental in northwestern Mexico) are commonly static, in the sense that there is no evidence for spatial migration of the magmatism with time, or intense deformation at intermediate crustal levels as a result of ballooning of large-scale stocks. The latter feature is commonly observed in coastal Cordilleran batholiths (e.g. the Sierra Nevada of California and the Peninsular Ranges batholith of Baja California), which undergo extensive structural and magmatic overturn and are characterized by spatial migration of the magmatism (e.g. Chen & Tilton, 1991); these arcs are also referred to as migrating arcs. Other parts of the Famatinian arc [e.g. the Sierra de Fiambalá mafic complex (DeBari, 1994)] may be equivalents of the coastal Cordilleran batholiths.

Few mid-crustal exposures of Cordilleran interior arcs are available for study; perhaps the best equivalents at similar paleo-depths within the arc are the early Cenozoic metamorphic core complexes of the northwestern USA, British Columbia and SE Alaska, which were segments of static interior arcs unroofed rapidly during extensional collapse of the northern Cordilleran system. The largest such exposure is the Central Gneiss Complex of British Columbia and SE Alaska (e.g. Hollister & Andronicos, 2006), which consists of tonalite sills intimately associated with metamorphosed migmatitic mafic and metasedimentary sequences. The entire central gneiss zone was subject to high-grade metamorphism and anatexis during Paleocene–Eocene times (e.g. Gehrels *et al.*, 2009) and ignited a high-flux magmatic event in the upper crust of that arc (Armstrong, 1988), one of the largest in the Cordillera (Ducea & Barton, 2007). A modern equivalent of the Cordilleran interior style of magmatism is the Altiplano–Puna region of the central Andes (de Silva & Gosnold, 2007).

The Famatinian exposure of Sierra Valle Fértil is similar to the gneiss domes of the northern Cordilleran interior in that it formed during a major static magmatic flare-up (~10 Myr) involving mantle-derived mafic magmas and a fertile metasedimentary crustal sequence that resulted in sill-like crustal magma bodies in the mid-crust and large-scale tonalitic and granodioritic intrusions at shallower levels (Fig. 14). The Sierra Valle Fértil section has no overprint of subsequent (unroofing-related or other) metamorphism (extension in the case of the gneiss domes), has outstanding exposures as a result of the local aridity, and exposes a tilted continuous section of the arc crust from mid-crustal (~22 km) to shallow levels of the paleo-arc section (Otamendi *et al.*, 2008). In addition, the presence of large unambiguously syn-arc mafic units and a rather uniform regional metasedimentary framework (e.g. the Puncoviscana Formation; Ježek *et al.*, 1985) provide simple end-members for understanding the physical and chemical processes involved in building this arc. Arguably, the Sierra Valle Fértil provides the simplest template of all exposed Cordilleran settings, allowing us to constrain the source zone of intermediate magmas emplaced near the Earth's surface.

CONCLUSIONS

Generation of intermediate tonalitic and dioritic magmas in the Famatinian arc crust is a multistage, multi-source process, involving at least two major components, one represented by juvenile mafic magmas and the other by intracrustal (mostly supracrustal) sedimentary rocks. This is consistent with the observation that the great majority of intermediate magmas in continental arcs contain an isotopically radiogenic crustal component (Sparks, 1986; Davidson *et al.*, 2005). The interplay between the juvenile mafic component (magmas or their crystallized products) and fertile metasedimentary lithologies can explain why significant volumes of intermediate magmas are generated rather rapidly at temperatures of 800–850°C in the deep levels of magmatic arcs (e.g. Annen & Sparks, 2002; Dufek & Bergantz, 2005; Annen *et al.*, 2006).

ACKNOWLEDGEMENTS

This paper benefited from careful reviews by Professors C. Annen, C. Barnes, and C. Miller, as well as the careful editorial handling of M. Wilson. This research was supported by FONCyT-Argentina grant PICTR20298/04 (to J.E.O. and G.I.V.) and an ExxonMobil grant (to M.N.D.). An Exchange Fellowship during the initial stages of this work was provided by a University of Huelva grant to J.E.O. Argentinean researchers are supported by CONICET.

SUPPLEMENTARY DATA

Supplementary data for this paper are available at *Journal of Petrology* online.

REFERENCES

Aceñolaza, F. G., Miller, H. & Toselli, A. J. (2000). The Pampean and Famatinian cycles—superposed orogenic events in the West Gondwana. *Zeitschrift für Angewandte Geologie, Sonderheft* **SH 1**, 337–344.

Allègre, C. J. & Minster, J. F. (1978). Quantitative models of trace element behavior in magmatic processes. *Earth and Planetary Science Letters* **38**, 1–25.

Anders, E. & Grevesse, N. (1989). Abundances of the elements—meteoritic and solar. *Geochimica et Cosmochimica Acta* **53**, 197–214.

Annen, C. & Sparks, R. S. J. (2002). Effects of repetitive emplacement of basaltic intrusions on thermal evolution and melt generation in the crust. *Earth and Planetary Science Letters* **203**, 937–955.

Annen, C., Blundy, J. D. & Sparks, R. S. J. (2006). The genesis of intermediate and silicic magmas in deep crustal hot zones. *Journal of Petrology* **47**, 505–539.

Arai, S. & Kida, M. (2000). Origin of fine-grained peridotite xenoliths from Iraya volcano of Batan Island, Philippines: deserpentinization or metasomatism at the wedge mantle beneath an incipient arc? *Island Arc* **9**, 458–471.

Armstrong, R. L. (1988). Mesozoic and early Cenozoic magmatic evolution of the Canadian Cordillera. In: Clark, S. P., Burchfiel, B. C. & Supper, J. (eds) *Processes in Continental Lithospheric Deformation: A Symposium to Honor John Rodgers. Geological Society of America, Special Papers* **218**, 55–91.

Astini, R. A. & Dávila, F. M. (2004). Ordovician back arc foreland and Ocloyic thrust belt development on the western Gondwana margin as a response to Precordillera terrane accretion. *Tectonics* **23**, TC4008, doi:10.1029/2003TC001620.

Atherton, M. P. (1993). Granite magmatism. *Journal of the Geological Society, London* **150**, 1009–1023.

Atherton, M. P. & Petford, N. (1993). Generation of sodium-rich magmas from newly underplated basaltic crust. *Nature* **362**, 144–146.

Barazangi, M. & Isacks, B. I. (1976). Spatial distribution of earthquakes and subduction of the Nazca plate beneath South America. *Geology* **4**, 686–692.

Barbero, L., Villaseca, C., Rogers, G. & Brown, P. E. (1995). Geochemical and isotopic disequilibrium in crustal melting: an insight from the anatectic granitoids from Toledo, Spain. *Journal of Geophysical Research* **100**, 15745–15765.

Barnes, C. G., Yoshinobu, A. S., Prestvik, T., Nordgulen, O., Karlsson, H. R. & Sundvoll, B. (2002). Mafic magma intraplating: anatexis and hybridization in arc crust, Bindal Batholith, Norway. *Journal of Petrology* **43**, 2171–2190.

Barton, M. D. (1996). Granitic magmatism and metallogeny of southwestern North America. *Transactions of the Royal Society of Edinburgh, Earth Sciences* **87**, 261–280.

Bea, F. (1996). Controls on the trace element composition of crustal melts. *Transactions of the Royal Society of Edinburgh, Earth Sciences* **87**, 33–41.

Beard, J. S. & Lofgren, G. E. (1991). Dehydration melting and water-saturated melting of basaltic and andesitic greestones and amphibolites at 1, 3, and 6·9 kb. *Journal of Petrology* **32**, 365–401.

Beard, J. S., Ragland, P. C. & Rushmer, T. (2004). Hydration crystallization reactions between anhydrous minerals and hydrous melt to yield amphibole and biotite in igneous rocks: Description and implications. *Journal of Geology* **112**, 617–621.

Beard, J. S., Ragland, P. C. & Crawford, M. L. (2005). Reactive bulk assimilation: A model for crust–mantle mixing in silicic magmas. *Geology* **33**, 681–684.

Bergantz, G. W. (1989). Underplating and partial melting: Implications for melt generation and extraction. *Science* **245**, 1093–1095.

Bohrson, W. A. & Spera, F. J. (2001). Energy-constrained open-system magmatic processes II: Aplication of energy-constrained assimilation–fractional crystallization (EC-AFC) model to magmatic systems. *Journal of Petrology* **42**, 1019–1041.

Caminos, R. J. (1979). Sierras Pampeanas Noroccidentales. Salta, Tucumán, Catamarca, La Rioja y San Juan. In: Leanza, E. F. (ed.) *Proceedings II Simposio de Geología Regional Argentina*. Córdoba: Academia Nacional de Ciencias, pp. 225–291.

Chappell, B. W. (1997). Compositional variation within granite suites of the Lachlan Fold Belt: its causes and implications for the physical state of granite magma. *Transactions of the Royal Society of Edinburgh, Earth Sciences* **88**, 159–170.

Chen, J. H. & Tilton, G. R. (1991). Applications of lead and strontium isotopic relationships to the petrogenesis of granitoid rocks, central Sierra Nevada batholith, California. *Geological Society of America Bulletin* **103**, 439–447.

Coira, B., Pérez, B., Flores, P., Kay, S. M., Woll, B. & Hanning, M. (1999). Magmatic sources and tectonic setting of Gondwana margin Ordovician magmas, northern Puna of Argentina and Chile. In: Ramos, V. & Keppie, J. (eds) *Laurentia–Gondwana Connections before Pangea. Geological Society of America, Special Papers* **336**, 145–170.

Collins, W. J. (1996). Lachlan Fold Belt granitoids: products of three-component mixing. *Transactions of the Royal Society of Edinburgh, Earth Sciences* **87**, 171–181.

Cox, K. G., Bell, J. D. & Pankhurst, R. J. (1979). *The Interpretation of Igneous Rocks*. London: George Allen & Unwin.

Davidson, J. P., Ferguson, K. M., Colucci, T. & Dungan, M. A. (1988). The origin and evolution of magmas from San Pedro–Pellado Volcanic Complex, S. Chile: multicomponent sources and open system evolution. *Contributions to Mineralogy and Petrology* **100**, 429–445.

Davidson, J. P., Hora, J. M., Garrison, J. M. & Dungan, M. A. (2005). Crustal forensics in arc magmas. *Journal of Volcanology and Geothermal Research* **140**, 157–170.

DeBari, S. (1994). Petrogenesis of the Fiambalá gabbroic intrusion, Northwestern Argentina, a deep crustal syntectonic pluton in a continental magmatic arc. *Journal of Petrology* **35**, 679–713.

DeBari, S. & Coleman, R. G. (1989). Examination of the deep levels of an island arc: evidence from the Tonsina ultramafic–mafic assemblage, Tonsina, Alaska. *Journal of Geophysical Research* **94**, 4373–4391.

DePaolo, D. J. (1981). A neodymium and strontium isotopic study of the Mesozoic calc-alkaline granitic batholiths of the Sierra Nevada and Peninsular Ranges, California. *Journal of Geophysical Research* **86**, 10470–10488.

DePaolo, D. J., Perry, F. V. & Baldridge, W. S. (1992). Crustal vs. mantle sources of granitic magmas: a two parameter model based on Nd isotopic studies. *Transactions of the Royal Society of Edinburgh, Earth Sciences* **83**, 439–446.

de Silva, S. L. & Gosnold, W. D. (2007). Episodic construction of batholiths: Insights from the spatiotemporal development of an ignimbrite flare-up. *Journal of Volcanology and Geothermal Research* **167**, 320–335.

Ducea, M. N. & Barton, M. D. (2007). Igniting flare-up events in Cordilleran arcs. *Geology* **35**, 1047–1050.

Ducea, M. N. & Saleeby, J. B. (1996). Buoyancy sources for a large, unrooted mountain range, the Sierra Nevada, California: evidence from xenolith thermobarometry. *Journal of Geophysical Research* **101**, 8226–8244.

Ducea, M. N. & Saleeby, J. B. (1998). The age and origin of a thick mafic ultramafic root from beneath the Sierra Nevada batholith. *Contributions to Mineralogy and Petrology* **133**, 169–185.

Ducea, M. N., Kidder, S. & Zandt, G. (2003). Arc compositions at mid-crustal depths: Insights from the Coast Ridge Belt, Santa Lucia Mountains, California. *Geophysical Research Letters* **30**, 1703 doi:10.1029/2002GL016297,2003.

Dufek, J. & Bergantz, G. W. (2005). Lower crustal magma genesis and preservation: a stochastic framework for the evaluation of basalt–crust interaction. *Journal of Petrology* **46**, 2167–2195.

Dungan, M. A. & Davidson, J. P. (2004). Partial assimilative recycling of the mafic plutonic roots of arc volcanoes: An example from the Chilean Andes. *Geology* **32**, 773–776.

Dunn, T. & Sen, C. (1994). Mineral/matrix partition coefficients for orthopyroxene, plagioclase, and olivine in basaltic to andesitic

systems: A combined analytical and experimental study. *Geochimica et Cosmochimica Acta* **58**, 717–733.

Eichelberger, J. C. (1978). Andesitic volcanism and crustal evolution. *Nature* **275**, 21–27.

Fanning, C. M., Pankhurst, R. J., Rapela, C. W., Baldo, E. G., Casquet, C. & Galindo, C. (2004). K-bentonites in the Argentine Precordillera contemporaneous with rhyolite volcanism in the Famatinian arc. *Journal of the Geological Society, London* **161**, 747–756.

Faure, G. (1986). *Principles Of Isotope Geochemistry*. New York: John Wiley.

Feeley, T. C., Clynne, M. A., Winer, G. S. & Grice, W. C. (2008). Oxygen isotope geochemistry of the Lassen Volcanic Center, California: resolving crustal and mantle contributions to continental arc magmatism. *Journal of Petrology* **49**, 971–997.

Frost, B. R., Barnes, C. G., Collins, W. J., Arculus, R. J., Ellis, D. J. & Frost, C. D. (2001). A geochemical classification for granitic rocks. *Journal of Petrology* **42**, 2033–2048.

Gamble, J. A., Wood, C. P., Price, R. C., Smith, I. E. M., Stewart, R. B. & Waight, T. (1999). A fifty year history of magmatic evolution on Ruapehu Volcano, New Zealand: verification of open system behaviour in an arc volcano. *Earth and Planetary Science Letters* **170**, 301–314.

García-Moreno, O., Castro, A., Corretgé, L. G. & El-Hmidi, H. (2006). Dissolution of tonalitic enclaves in ascending hydrous granitic magmas: an experimental study. *Lithos* **89**, 245–258.

Garrido, C. J., Bodinier, J.-L., Burg, J.-P., Zilinger, G., Hussain, S. S., Dawood, H., Chaudhry, M. N. & Gervilla, F. (2006). Petrogenesis of mafic garnet granulite in the lower crust of the Kohistan paleo-arc complex (Northern Pakistan): implications for intra-crustal differentiation of island arcs and generation of continental crust. *Journal of Petrology* **47**, 1873–1914.

Gehrels, G. E., Rusmore, M., Woodsworth, G., Andronicos, C. L., Hollister, L., Patchett, P. J., Ducea, M. N., Butler, R., Klepeis, K., Davidson, C., Friedman, R., Haggart, J., Mahoney, B., Crawford, W., Pearson, D. & Girardi, J. (2009). U–Th–Pb geochronology of the Coast Mountains Batholith in north–coastal Brititsh Columbia: constraints on age, petrogenesis, and tectonic evolution. *Geological Society of America Bulletin* (in press).

Gill, J. (1981). *Orogenic Andesites and Plate Tectonics*. Berlin: Springer.

Gray, C. M. (1984). An isotopic mixing model for the origin of granitic rocks in southeastern Australia. *Earth and Planetary Science Letters* **70**, 47–60.

Greene, A. R., DeBari, S., Kelemen, P. B., Blusztajn, J. & Clift, P. (2006). A detailed geochemical study of island arc crust: the Talkeetna Arc section, south–central Alaska. *Journal of Petrology* **47**, 1051–1093.

Gromet, P. & Silver, L. T. (1987). REE variations across the Peninsular Ranges Batholith: implications for batholith petrogenesis and crustal growth in magmatic arcs. *Journal of Petrology* **28**, 75–125.

Grove, T. L. & Kinzler, R. J. (1986). Petrogenesis of andesites. *Annual Review of Earth and Planetary Sciences* **14**, 417–454.

Hildreth, W. & Moorbath, S. (1988). Crustal contributions to arc magmatism in the Andes of Central Chile. *Contributions to Mineralogy and Petrology* **98**, 455–489.

Hollister, L. S. & Andronicos, C. L. (2006). Formation of new continental crust in Western British Columbia during transpression and transtension. *Earth and Planetary Science Letters* **249**, 29–38.

Holtz, F., Johannes, W., Tamic, N. & Behrens, H. (2001). Maximum and minimum water contents of granitic melts generated in the crust: a reevaluation and implications. *Lithos* **56**, 1–14.

Jackson, M. D., Cheadle, M. J. & Atherton, M. P. (2003). Quantitative modeling of granitic melt generation and segregation in the continental crust. *Journal of Geophysical Research* **108**(B7), 2332, doi:10.1029/2001JB001050, 2003.

Jagoutz, O., Müntener, O., Ulmer, P., Pettke, T., Burg, J., Dawood, H. & Hussain, S. (2007). Petrology and mineral chemistry of lower crustal intrusions: the Chilas Complex, Kohistan (NW Pakistan). *Journal of Petrology* **48**, 1895–1953.

Ježek, P., Willner, A. P., Aceñolaza, F. G. & Miller, H. (1985). The Puncoviscana trough—a large basin of Late Precambrian to Early Cambrian age on the Pacific edge of the Brazilian shield. *Geologische Rundschau* **74**, 573–584.

Kidder, S. & Ducea, M. N. (2006). High temperatures and inverted metamorphism in the schist of Sierra de Salinas, California. *Earth and Planetary Science Letters* **241**, 422–437.

Klein, M., Stosch, H.-G. & Seck, H. A. (1997). Partitioning of high field-strength and rare-earth elements between amphibole and quartz-dioritic to tonalitic melts: an experimental study. *Chemical Geology* **138**, 257–271.

Kretz, R. (1983). Symbols for rock-forming minerals. *American Mineralogist* **68**, 277–279.

Langmuir, C. H., Vocke, R. D., Hanson, G. N. & Hart, S. R. (1978). A general mixing equation with applications to Icelandic basalts. *Earth and Planetary Science Letters* **37**, 380–392.

Lee, C.-T. A., Cheng, X. & Horodyskyj, U. (2006). The development and refinement of continental arcs by primary basaltic magmatism, garnet pyroxenite accumulation, basaltic recharge and delamination: insights from the Sierra Nevada, California. *Contributions to Mineralogy and Petrology* **151**, 222–242.

Le Maitre, R. W. (1979). A new generalized petrological mixing model. *Contributions to Mineralogy and Petrology* **71**, 133–137.

Le Maitre, R. W., Bateman, P., Dudek, A., Keller, J., Lameyre, J., Le Bas, M. J., Sabine, P. A., Schmid, R., Sørensen, S., Streckeisen, A., Woolley, A. R. & Zanettin, B. (1989). *A Classification of Igneous Rocks and Glossary of Terms*. Oxford: Blackwell Scientific.

Mannhein, R. & Miller, H. (1996). Las rocas volcánicas y subvolcánicas eopaleozoicas del Sistema de Famatina. In: Aceñolaza, F. G., Miller, H. & Toselli, A. (eds) *Geología del Sistema de Famatina. Münchner Geologische Hefte* **A19**, 159–186.

Mirré, J. C. (1976). *Descripción Geológica de la Hoja 19e, Valle Fértil, Provincias de San Juan y La Rioja*. Buenos Aires: Servicio Geológico Nacional, pp. 1–70.

Muir, R. J., Ireland, T. R., Weaver, S. D., Bradshaw, J. D., Evans, J. A., Eby, G. N. & Shelley, D. (1998). Geochronology and geochemistry of a Mesozoic magmatic arc system, Fiordland, New Zealand. *Journal of the Geological Society, London* **155**, 1037–1053.

Otamendi, J. E., Tibaldi, A. M., Vujovich, G. I. & Viñao, G. A. (2008). Metamorphic evolution of migmatites from the deep Famatinian arc crust exposed in Sierras Valle Fértil–La Huerta, San Juan, Argentina. *Journal of South American Earth Sciences* **25**, 313–335.

Otamendi, J. E., Vujovich, G. I., de la Rosa, J. D., Tibaldi, A. M., Castro, A., Martino, R. D. & Pinotti, L. P. (2009). Geology and petrology of a deep crustal zone from the Famatinian paleo-arc, Sierras Valle Fértil–La Huerta, San Juan, Argentina. *Journal of South American Earth Sciences*, doi:10.1016/j.jsames.2008.11.007.

Pankhurst, R. J., Rapela, C. W., Saavedra, J., Baldo, E. G., Dahlquist, J., Pascua, I. & Fanning, C. M. (1998). The Famatinian magmatic arc in the central Sierras Pampeanas: an Early to Mid-Ordovician continental arc on the Gondwana margin. In: Pankhurst, R. J. & Rapela, C. W. (eds) *The Proto-Andean Margin of Gondwana. Geological Society, London, Special Publications* **142**, 343–368.

Pankhurst, R. J., Rapela, C. W. & Fanning, C. M. (2000). Age and origin of coeval TTG, I- and S-type granites in the Famatinian belt of NW Argentina. *Transactions of the Royal Society of Edinburgh, Earth Sciences* **91**, 151–168.

Parkinson, I. J., Arculus, R. J. & Eggins, S. M. (2003). Peridotite xenoliths from Grenada, Lesser Antilles Island Arc. *Contributions to Mineralogy and Petrology* **146**, 241–262.

Patiño Douce, A. E. (1995). Experimental generation of hybrid silicic melts by reaction of high-Al basalt with metamorphic rocks. *Journal of Geophysical Research* **100**, 15623–15639.

Patiño Douce, A. E. (1999). What do experiments tell us about the relative contributions of crust and mantle to the origin of granitic magmas? In: Castro, A., Fernández, C. & Vigneresse, J. L. (eds) *Understanding Granites: Integrating New and Classical Techniques Geological Society, London, Special Publications* **168**, 55–75.

Pickett, D. A. & Saleeby, J. B. (1993). Thermobarometric constraints on the depth of exposure and conditions of plutonism and metamorphism at deep levels of the Sierra Nevada batholith, Tehachapi Mountains, California. *Journal of Geophysical Research* **98**, 609–629.

Rapela, C. W., Coira, B., Toselli, A. & Saavedra, J. (1992). The Lower Paleozoic magmatism of southwestern Gondwana and the evolution of Famatinian orogene. *International Geology Review* **34**, 10081–1142.

Reiners, P. W., Nelson, B. K. & Nelson, S. W. (1996). Evidence for multiple mechanisms of crustal contamination of magma from compositionally zoned plutons and associated ultramafic intrusions of the Alaska Range. *Journal of Petrology* **37**, 261–292.

Rollinson, H. R., 1993. *Using Geochemical Data: Evaluation, Presentation, Interpretation*. London: Longman.

Rudnick, R. L. & Fountain, D. M. (1995). Nature and composition of the continental crust: A lower crustal perspective. *Review of Geophysics* **33**, 267–309.

Rushmer, T. (1991). Partial melting of two amphibolites: contrasting results under fluid-absent conditions. *Contributions to Mineralogy and Petrology* **107**, 41–59.

Saleeby, J. B. (1990). Progress in tectonic and petrogenetic studies in an exposed cross-section of young (*c.* 100 Ma) continental crust, southern Sierra Nevada, California. In: Salisbury, M. H. & Fountain, D. M. (eds) *Exposed Crustal Sections of the Continental Crust*. Norwell, MA: Kluwer Academic, pp. 137–158.

Sawyer, E. W. (1987). The role of partial melting and fractional crystallization in determining discordant migmatite leucosome compositions. *Journal of Petrology* **28**, 445–473.

Sawyer, E. W. (1991). Disequilibrium melting and the rate of melt–residuum separation during migmatization of mafic rocks from the Grenville Front, Quebec. *Journal of Petrology* **32**, 701–738.

Sawyer, E. W. (1996). Melt segregation and magma flow in migmatites: Implications for the generation of granitic magmas. *Transactions of the Royal Society of Edinburgh, Earth Sciences* **87**, 85–94.

Silver, L. T. & Chappell, B. W. (1988). The Peninsular Ranges Batholith: An insight into the evolution of the Cordilleran batholiths of southwestern North America. *Transactions of the Royal Society of Edinburgh, Earth Sciences* **79**, 105–121.

Sisson, T. W., Ratajeski, K., Hankins, W. B. & Glazner, A. F. (2005). Voluminous granitic magmas from common basaltic sources. *Contributions to Mineralogy and Petrology* **148**, 635–661.

Skjerlie, K. P. & Patiño Douce, A. E. (1995). Anatexis on interlayered amphibolite and pelite at 10 kbar: effect of diffusion of major components on phase relations and melt fraction. *Contributions to Mineralogy and Petrology* **122**, 62–78.

Sparks, R. S. J. (1986). The role of crustal contamination in magma evolution through geological time. *Earth and Planetary Science Letters* **78**, 211–223.

Stair, K., Ducea, M., Otamendi, J., Gerhels, G. & Bergantz, G. (2007). U–Pb zircon plutonic emplacement and metamorphic ages from a tilted crustal section of the Famatinian arc, northwestern Argentina: Petrologic and regional tectonic implications. In: Arizona Geological Society (ed) *Ore & Orogenesis 2007*. Abstracts, 245. Arizona Geological Society, Tucson.

Tatsumi, Y. & Eggins, S. (1995). *Subduction Zone Magmatism*. Oxford: Blackwell Scientific.

Tepper, J. H., Nelson, B. K., Bergantz, G. W. & Irving, A. J. (1993). Petrology of the Chilliwack batholith, North Cascades, Washington: generation of calc-alkaline granitoids by melting of mafic lower crust with variable water fugacity. *Contributions to Mineralogy and Petrology* **110**, 448–499.

Toselli, A. J., Durand, F. R., Rossi de Toselli, J. N. & Saavedra, J. (1996). Esquema de evolución geotectónica y magmática Eopaleozoica del Sistema de Famatina y sectores de Sierras Pampeanas. In: Ramos, V. (ed.) *Proceedings XIII Congreso Geológico Argentino* **5**, 443–462, Asociación Geológica Argentina, Buenos Aires.

Vigneresse, J. L., Barbey, P. & Cuney, M. (1996). Rheological transition during partial melting and crystallization with application to felsic magma segregation and transfer. *Journal of Petrology* **37**, 1579–1600.

Vujovich, G. I., Godeas, M., Marín, G. & Pezzutti, N. (1996). El complejo magmático de la Sierra de La Huerta, provincia de San Juan. In: Ramos, V. (ed.) *Proceedings XIII Congreso Geológico Argentino* **3**, 465–475, Asociación Geológica Argentina, Buenos Aires.

Wasserburg, G. J., Jacobsen, S. B., DePaolo, D. J., McCulloch, M. T. & Wen, T. (1981). Precise determination of Sm/Nd ratios, Sm and Nd isotopic abundances in standard solutions. *Geochimica et Cosmochimica Acta* **45**, 2311–2323.

Whitney, J. A. (1975). The effects of pressure, temperature, and X_{H2O} on phase assemblage in four synthetic rock compositions. *Journal of Geology* **83**, 1–31.

Williams, M. K., Hanmer, S., Kopf, C. & Darrach, M. (1995). Syntectonic generation and segregation of tonalitic melts from amphibolite dikes in the lower crust, Striding–Athabasca mylonite zone, northern Saskatchewan. *Journal of Geophysical Research* **100**, 15717–15734.

Zandt, G., Gilbert, H., Owens, T. J., Ducea, M., Saleeby, J. & Jones, C. H. (2004). Active foundering of continental arc root beneath the southern Sierra Nevada in California. *Nature* **431**, 41–46.

Zeng, L., Saleeby, J. B. & Ducea, M. (2005). Geochemical characteristics of crustal anatexis during the formation of migmatite at the Southern Sierra Nevada, California. *Contributions to Mineralogy and Petrology* **150**, 486–402.